universität
wien

DIPLOMARBEIT

Titel der Diplomarbeit

Entangled Photon Experiments with a Fast Interferometric Switchable Beam Splitter

angestrebter akademischer Grad

Magister der Naturwissenschaften (Mag. rer.nat.)

Verfasser:	Stefan Zotter
Matrikel-Nummer:	0400384
Studienrichtung (lt. Studienblatt):	411
Betreuerin / Betreuer:	o.Univ.-Prof. Dr. DDr.h.c. Anton Zeilinger

Wien, am   23.6.2009

Contents

1. Introduction

This thesis describes experiments which deal with two fundamental principles of Quantum Mechanics, entanglement and complementarity. Entanglement denotes the phenomenon that two or even more particles can be in a superposition and therefore the single system is highly correlated to its partners even though they are spatially separated. And complementarity, which is related to the Heisenberg Uncertain Principle, means that two properties of a quantum system e.g. momentum and position or particle and wave nature, can not be observed simultaneously with arbitrary precision. Both principles led to one of the most fruitful discussions in modern physics. One of the most famous papers in this time was the EPR paper (Einstein - Podolsky - Rosen) in 1935 [1]. Einstein didn't liked the idea that the result of an experiment would depend on the measurement device nor that it could depend on the result of another measurement which is spatially separated. He thought that Quantum Mechanics must be incomplete because it conflicts with his *local realistic world* in which *"[...] the universe exists "out there" independent of all acts of observation."* [2]. In 1964 J. Bell [3] showed that in some cases, local realistic theories are in contradiction with Quantum Mechanics. The whole discussion led to a new field in modern physics, called Quantum Information Science which amazes us with fundamentally new ways of communication and computation. Things like quantum teleportation and quantum cryptography are not only theoretical issues but are also known by the public society and led to new technologies that will change our communication systems in the future.

Here I present a polarization independent ultrafast interferometric switchable beam splitter, which can be used for several experiments. It consists of a Mach-Zehnder interferometer with one Pockels cell or Electro Optical Modulator (EOM) in each arm, which, vary the phase of a transmitted beam by an electric field induced birefringence in a crystal. The splitting ratio of the effective beam splitter, can be tuned by changing the applied voltage. In this thesis I want to focus on the fundamental concepts of quantum mechanics and therefore we show a complementarity relation of a two particle system and finally we want to realize the "delayed-choice entanglement swapping experiment" introduced by A. Peres [4, 5].

2. Motivation

The motivation for this thesis is to illustrate some of the fundamental aspects of Quantum Physics. In contradiction to Classical Mechanics, which describes most of our every day life and is very intuitive, Quantum Mechanics is more fundamental and explains the behavior of atoms, electrons, the interaction of matter and electromagnetic radiation, the wave-particle nature of matter and light and many other things. But its principles are sometimes very counterintuitive and provide us with many seemingly paradox situations, such as complementarity or "spooky action at distance". But according to A. Peres, these paradoxes do not arise if *[...] the correctness of quantum mechanics is firmly believed."* [4]

2.1. Wave-Particle Duality

The wave-particle duality is one of the fundamental principles of Quantum Physic and tells us that every matter or energy is able to exhibit particle and wave nature depending on the measurement apparatus. It can easily be understood by discussing Young's double-slit experiment (see figure 2.1). In the classical picture this can be explained by interfering
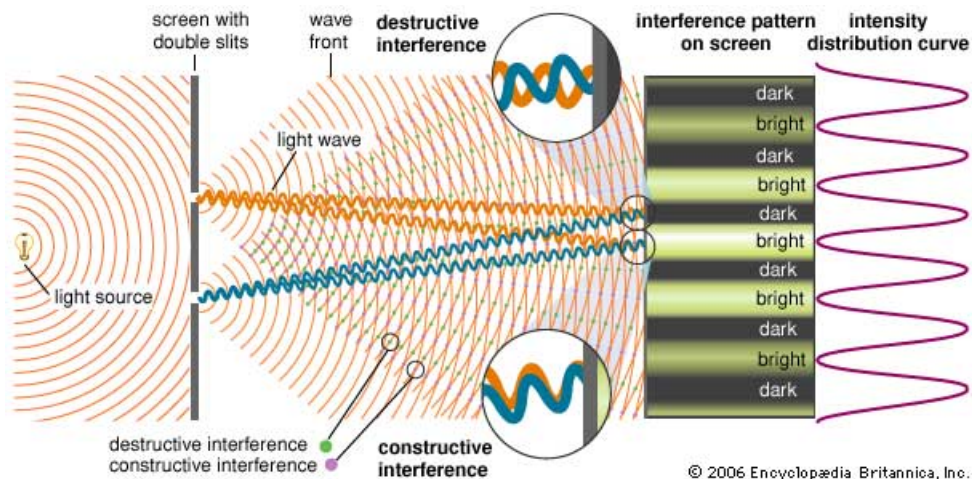

Figure 2.1.: *Young's double-slit experiment. Coherent light is sent on a screen with two holes. The two waves are able to interfere constructively or destructively with each other depending on their phase difference. Picture taken from http://www.britannica.com/EBchecked/topic/654179/Youngs-experiment.*

waves. But what happens if the light source is attenuated such that only one photon at a time passes through the double slit? Even in this case one will observe the typical interference pattern after integrating over a sufficient number of photons. This experiment was not only performed with single photons, but also with electrons [6], neutrons [7], atoms [8] and even massive C60 molecules [9] and proofs the wave nature of massive particles. But if the experimenter decides to block one slit, the interference pattern will automatically vanish. So the question whether the quantum object behaves as a single particle or as a wave depends on the measurement apparatus.

Another good example for this circumstance is the Mach-Zehnder interferometer (see figure 2.2). In this type of interferometer light is split on a first beam splitter and recombined by two mirrors on a second beam splitter. Again one will observe a phase dependent interference pattern between the two output modes, even if only one photon passes the interferometer after the other. Like in the double-slit experiment it is impossible to say "which-way" the photon has taken inside the interferometer. But if one takes out the second beam splitter we will not see any interference fringes and each detector has equal probability $p = 0,5$ to register a photon, independent of the phase shift inside the Mach-Zehnder. In this configuration we know exactly which path the photons have traveled.

2.2. Delayed-Choice

John Wheeler pushed this phenomenon even further by introducing his famous "delayed-choice gedankenexperiment". He proposed to *"[...] make the decision whether to put the final half-silvered mirror in place or to take it out at the very last picosecond, after the photon has already accomplished its travel. In this sense, we have a strange inversion of the normal order of time. We, now, by moving the mirror in or out have an unavoidable effect on what we have a right to say about the already past history of that photon."* [2].

This Gedankenexperiment was realized in several experiments with photons [10, 11, 12] and even within an atom-interferometer [13]. A schematic picture of the delayed-choice experiment by Hellmuth et al. [10] can be seen in figure 2.2. A single photon enters the first beam splitter of a Mach-Zehnder interferometer and is coupled into two delay fibers. An additional Pockels Cell is placed in one arm which acts as a half-wave plate and rotates the polarization of the incoming photon by 90° if a high voltage is applied. The Pockels Cell is followed by a Glan-Thompson prism which deflects the beam if the polarization is rotated and transmits the photon if the polarization is preserved. Afterwards the two arms are recombined on a second beam splitter and detected with photomultipliers (PM). So the decision whether to open or close one arm of the interferometer can be done after the photon has already past the first beam splitter.
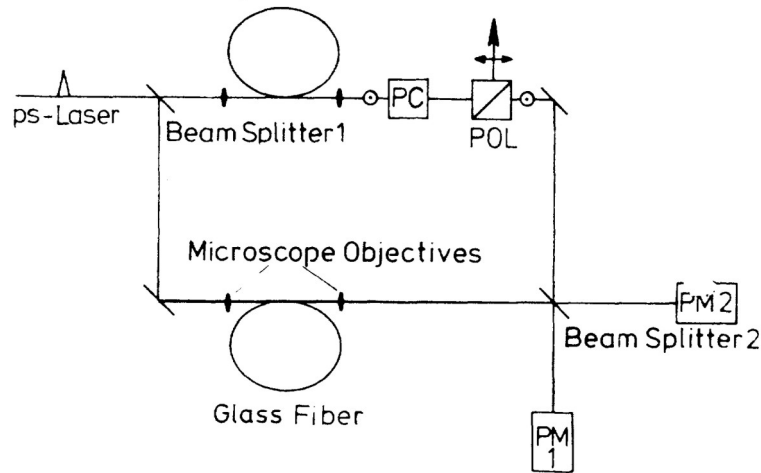
Figure 2.2.: *A schematic picture of the first Delayed-Choice Experiment performed by Hellmuth et al. [10]. A single photon coming from a picosecond Laser (ps-Laser) enters a Mach-Zehnder interferometer. After the first beam splitter, the photon is coupled into a delay fiber (one in each arm). A Pockels Cell (PC) is placed in one arm of the interferometer, which rotates the polarization of the photon by 90° if a high voltage is applied. A Glen-Thompson prism (POL) transmits the photon if the polarization is preserved or deflects it if the polarization is rotated by the Pockels Cell. After recombining the two arms on the second beam splitter, the photon is detected with photomultipliers (PM). Picture taken from the original paper.*

2.3. Entanglement and the EPR-Paradox

The superposition principle, which lies at the heart of Quantum Mechanics, can be generalized to two or even more particles. This was introduced by E. Schrödinger in 1935 [14], who named this phenomenon "Verschränkung", which was translated to the english word "entanglement".

Based on the example of an entangled state Einstein, Podolsky and Rosen (EPR [1]) tried to show that Quantum Mechanics is incomplete. They argued that Quantum Mechanics is in contradiction with their assumptions about a physical theory. Their contention was based on the following terms:

- **Completeness**: *"Every element of the physical reality must have a counterpart in the physical theory."* [1]

- **Reality**: *"If, without in any way disturbing a system, we can predict with certainty (i.e. with probability equal to unity) the value of a physical quantity, then there exists an element of physical reality corresponding to this physical quantity".* [1]

- **Locality**: *"... the real factual situation of system S1 is independent of what is done*

with system S2, which is spatially separated from the former". [15]

They used the example of a two-particle entangled system (momentum and position). The sum of the momenta and the difference of the positions is well defined for the two-particle system, but it is completely random for the individual one. If they are space-like separated and if an observer decides to measure e.g. the momentum of particle 1, he would immediately gain knowledge about the momentum of the second one. Based on their assumption that information cannot travel faster than light from one particle to the other, they concluded that the information about the momentum of the second particle must have been part of physical reality. They also stated that the observer could decide to measure the position of particle 1 instead of the momentum and that the information about the position of particle 2 must also been part of physical reality. Therefore both properties of the second particle must be part of physical reality. In this way EPR claimed that one could gain precise knowledge about two non commuting observables (e.g. momentum and position). This is in direct contradiction to Heisenberg's uncertainty principle and therefore Quantum Mechanics must be incomplete.

In his famous paper in 1935 [16], Niels Bohr replied to EPR's argumentation by criticizing their *"Reality"* assumption. He picks up their argument *"without in any way disturbing a system"* by saying: *"Of course there is in a case like that just considered no question of a mechanical disturbance of the system under investigation during the last critical stage of the measuring procedure. But even at this stage there is essentially the question of an influence on the very conditions which define the possible types of predictions regarding the future behavior of the system"* [16]. Therefore EPR's *"Reality"* assumption is wrong and their conclusion that Quantum Mechanics is incomplete is not justified.

If one wants to hold on to Einsteins *local, realistic world*, one needs to explain the correlations between entangled particles. *Local Hidden Variable Theories* are an attempt to explain that the outcome of every possible measurement on a particle is determined by a set of hidden variables. These theories try to explain the Quantum Mechanical predictions from a more intuitional local realistic point of view.

2.4. Bell's Inequality

Before John Bell published his famous paper in 1964 [3], most physicists believed that the formulation of a Hidden Variable Theory is difficult but possible. The problem was not solved but at least there was a potential solution. But then Bell showed a discrepancy between those two theories by introducing an inequality which is obeyed for a Local Hidden Variable Theory and violated by Quantum Mechanics.

A very popular form of Bell's inequality is the Clauser, Horn, Shimony and Holt (CHSH)

inequality [17]. It is written as

$$S = |E(a,b) + E(a,b')| + |E(a',b) - E(a',b')| \leq 2 \tag{2.1}$$

where $E(a,b)$ denotes the expectation value for the correlation measurement on particle 1 and 2. a and b are the analyzer settings. For particles in a polarization entangled state this expectation value is calculated as $E(a,b) = -\cos(a-b)$ in the ideal case. If the entangled state has the form $|\Psi^-\rangle = \frac{1}{\sqrt{2}}(|H\rangle_1|V\rangle_2 - |V\rangle_1|H\rangle_2)$, Quantum Mechanics predicts a maximum value for $S = 2\sqrt{2}$ which clearly violates the classical hidden variable limit[1]. Bell's inequalities have been violated experimentally for many different entangled systems e.g. photons [18, 19, 20], ions [21] and many others.

2.5. Quantum State Teleportation

Quantum State Teleportation was introduced by Bennet et al. in 1993 [22] and experimentally realized by Bouwmeester et al. in 1997 [23]. It allows to transfer the quantum state of one system to another one. The original quantum state of the teleported particle gets erased[2] while the receiver carries the information of the original one.

A schematic diagram of a Teleportation protocol can be seen in figure 2.3. Photon 1 is initially in an unknown quantum state $|\Psi\rangle = (\alpha|H\rangle_1 + \beta|V\rangle_1)$ whereas photons 2 and 3 are in one of the four maximal entangled Bell-states, which look like:

$$\begin{aligned} |\Psi^\pm\rangle &= \frac{1}{\sqrt{2}}(|H\rangle_1|V\rangle_2 \pm |V\rangle_1|H\rangle_2) \\ |\Phi^\pm\rangle &= \frac{1}{\sqrt{2}}(|H\rangle_1|H\rangle_2 \pm |V\rangle_1|V\rangle_2) \end{aligned} \tag{2.2}$$

Without loss of generality we assume that they are prepared in a $|\Psi^-\rangle_{23} = \frac{1}{\sqrt{2}}(|H\rangle_2|V\rangle_3 - |V\rangle_2|H\rangle_3)$ state. Then the state of the whole system can be written as

$$|\Psi\rangle_{total} = |\Psi\rangle_1 \otimes |\Psi^-\rangle_{23} = (\alpha|H\rangle_1 + \beta|V\rangle_1) \otimes \frac{1}{\sqrt{2}}(|H\rangle_2|V\rangle_3 - |V\rangle_2|H\rangle_3) \tag{2.3}$$

By performing a Joint Measurement (called Bell-state measurement, see appendix C) on photons 1 and 2, Alice projects the input state $|\Psi\rangle$ onto photon 3. The final state looks

---

[1]The measurement angles have to be $a = 0°, 45°$ and $b = 22,5°, 67,5°$.

[2]The state of the original particle has to be destroyed because it gets entangled with particle 2 after the Bell-state Measurement.
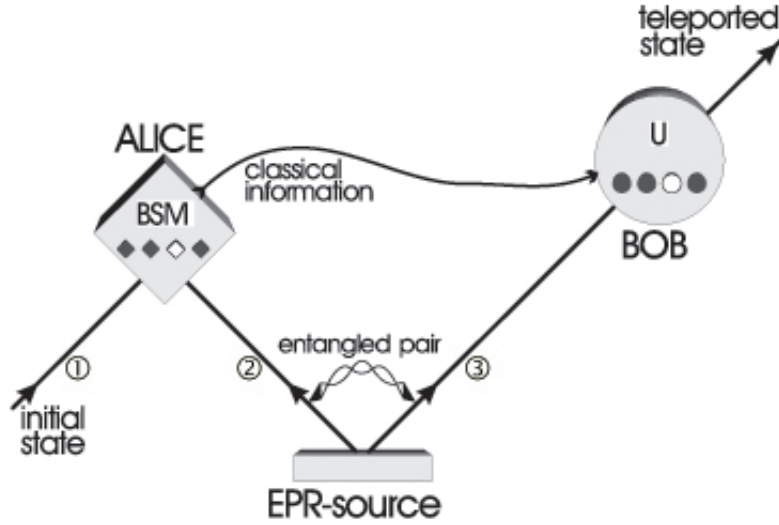
Figure 2.3.: *A schematic diagram of Quantum State Teleportation Protocol. The initial quantum state of photon 1 is transfered to photon 3. In order to achieve this, Alice has to perform a Bell-state Measurement on photons 1 and 2 and send Bob the result of her measurement via a classical channel. With this classical information Bob is able to reconstruct the original input state of photon 1 by performing a unitary transformation on photon 3. For details see text. Picture taken from [24]*

like

$$|\Psi\rangle_{total} = \frac{1}{\sqrt{2}}[(\alpha|H\rangle_3 - \beta|V\rangle_3)|\Psi^+\rangle_{12} - (\alpha|H\rangle_3 + \beta|V\rangle_3)|\Psi^-\rangle_{12} - (\alpha|V\rangle_3 + \beta|H\rangle_3)|\Phi^+\rangle_{12} + (\alpha|V\rangle_3 - \beta|H\rangle_3)|\Phi^-\rangle_{12}]$$

(2.4)

Here photons 2 and 3 are expressed in terms of the four Bell-states. One can see that photons 2 and 3 are no longer entangled, but now photons 1 and 2 are in one of the four maximal entangled states.

If Alice finds photons 2 and 3 in a $|\Psi^-\rangle$ state then Bob's photon will be in the state $-(\alpha|H\rangle_3 + \beta|V\rangle_3)$ which is identical with the input except for the $-$ sign. Note that Bob has to know which Bell-state Alice has detected between photons 1 and 2, because he has to perform an unitary transformation in order to reconstruct the original input state. If he does not wait for this classical information, his photon will be in one of the four Bell-states and hence act as a perfect mixed state. This assures that special relativity is not violated by the Quantum Teleportation Protocol. Even if photon 3 is projected into a specific state instantaneously during the Bell State Measurement of 1 and 2, Bob has to wait for Alice's message until he can reconstruct the input state. Therefore no information can be transported faster than the speed of light in the teleportation protocol.

2.6. Entanglement Swapping

Entanglement swapping is the generalization of quantum teleportation. Instead of one entangled photon pair and an undefined input photon, entanglement swapping works with 2 entangled photon pair sources (see figure 2.4). The initial entanglement between photons a, b and c, d is swapped to photons a and d by performing a Bell-state measurement between photons b and c. This experimental scheme was proposed by M. Zukowski et al. in 1993 [25] and experimentally realized by J. W. Pan et al. in 1998 [26].
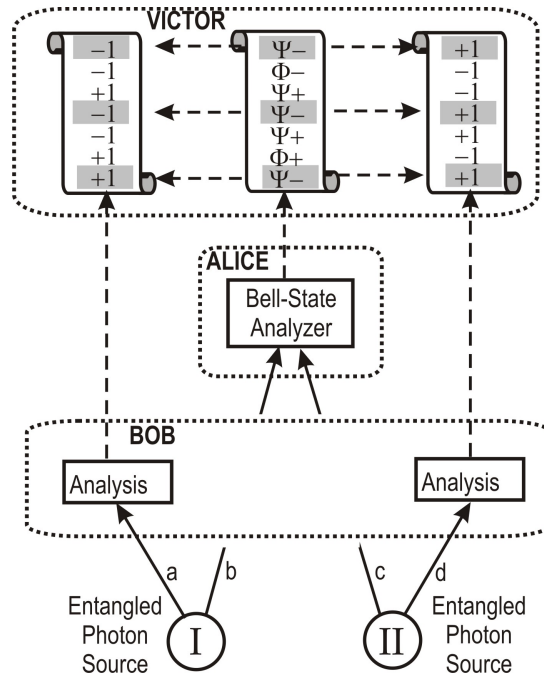
Figure 2.4.: *The principle of entanglement swapping. Photons b and c from two independent entangled photon pairs are projected onto an entangled state via a Bell-state measurement. In this way photons a and d become entangled although they have never interacted with each other in the past. Bob is free to choose the polarization angles but both, Alice and Bob, have to hand over their measurement results to a third party named Victor. He puts Bob's results into a subset according to Alice's results and checks if photons a and d became entangled. Picture taken from [27].*

The initial state can be written as[3]

$$|\Psi\rangle_{total} = |\Psi^-\rangle_{ab} \otimes |\Psi^-\rangle_{cd} \qquad (2.5)$$

---

[3]Note that any of the other four maximally entangled Bell-states (see equation3.3) is also valid in this case.

This can be rewritten in the basis of Bell-states

$$|\Psi\rangle_{total} = \frac{1}{2}[|\Phi^-\rangle_{ad}|\Phi^-\rangle_{bc} - |\Phi^+\rangle_{ad}|\Phi^+\rangle_{bc} - |\Psi^-\rangle_{ad}|\Psi^-\rangle_{bc} + |\Psi^+\rangle_{ad}|\Psi^+\rangle_{bc}] \qquad (2.6)$$

From this result one can see that it does not even matter onto which state Alice projects, photons a and d will be maximally entangled in the corresponding Bell-state.

2.7. Delayed-Choice Entanglement Swapping

An experiment which combines the idea of delayed-choice and entanglement swapping was introduced by A. Peres. He proposed *"[...] an even more paradoxical experiment, where entanglement is produced a posteriori, after the entangled particles have been measured and may no longer exist."* [4]. The setup for this experiment is the same as in figure 2.4 but this time photons a and d are measured and detected before the Bell-state measurement is performed on photons b and c. This seems paradoxical because the measurement that projects photons a and d onto an entangled state is performed after they have already been detected and do not longer exist. *"How can the appearance of entanglement arise in these circumstances? The point is that it is meaningless to assert that two particles are entangled without specifying in which state they are entangled [...]"* [4]. T. Jennewein et al. said that *"Therefore, this result indicates that the time ordering of the detection events has no influence on the results and strengthens the argument of Peres [4]: This paradox does not arise if the correctness of quantum mechanics is firmly believed."* [28]. In their paper they also showed the first experimental realization of Peres Gedankenexperiment.

In another proposal T. Jennewein et al. [29] extended the "delayed-choice entanglement swapping experiment" in the following way. A schematic picture of their gedankenexperiment can be seen in figure 2.5. Alice and Bob detect photons a and d whereas Victor performs a Bell-state measurement on photons b and c, like in the Peres experiment. But this time Victor is free to choose what kind of measurement he wants to perform. *"Instead of a Bell-measurement he could also measure the polarization of these photons individually which would result in a well defined polarization for photons a and d, i.e. a separable product state."* [29]. The choice whether to project photons a and d or to leave them in a separable product state could be done randomly by a quantum random number generator (QRNG) and also after these photons have already been registered.

Like in the entanglement swapping experiment we start of with two polarization-entangled photon pairs. Source 1 emits into spatial mode a and b whereas the entangled photons from source 2 can be found in mode c and d. The polarization from photons a and d is measured immediately afterwards. The photons in mode b and c are send to a Mach-Zehnder interferometer with a phase shifter in one arm. The calculations in chapter 6 will show
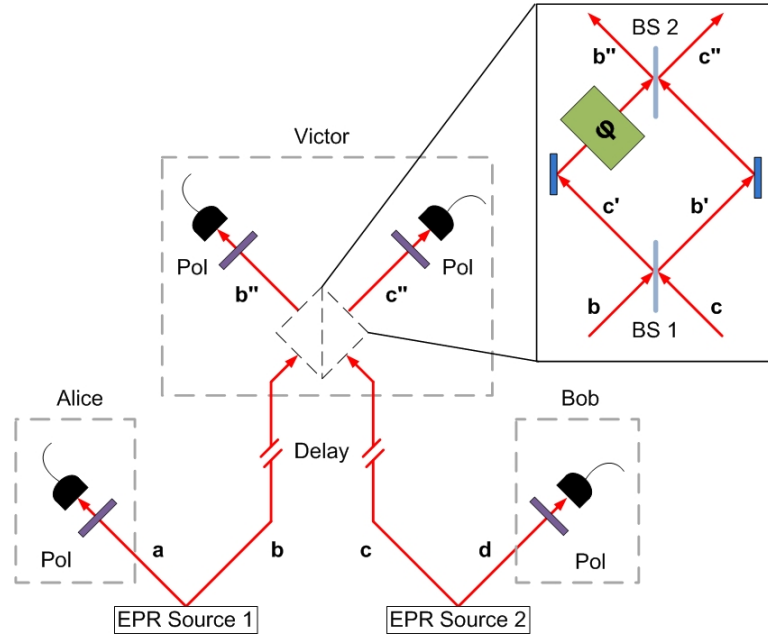
Figure 2.5.: *A schematic diagram of a proposed "delayed-choice entanglement swapping experiment". Two Einstein-Podolsky-Rosen sources emit polarization-entangled photon pairs between spatial mode a,b and c,d. The polarization of photons a and d is measured immediately afterwards. This can be done by a polarizer or a polarizing beam splitter. Photons b and c are delayed before entering a Mach-Zehnder interferometer. By tuning the phase inside the interferometer between $\varphi = \frac{\pi}{2}$ and $\varphi = 0$, one can decide to perform a Bell-state measurement or not. In the first case photons a and d become entangled, although they have never interacted with each other in the past and do not longer exist. To show the entanglement between both photons, one could violate a CHSH inequality for example. In the second case, photons b and c pass through the interferometer and do not interact with each other. Therefore photons a and d remain in a complete separable state. Picture adopted and changed from [29].*

that by switching the phase inside the interferometer between $\varphi = \frac{\pi}{2}$ and $\varphi = 0$ one can actively decide to perform a Bell-state measurement or to let the photons pass through the interferometer and keep them separated. Victor has to tell Alice and Bob in which case he inserted the beam splitter and therefore projected photons a, d onto an entangled state or when he decided to keep photons b'', c'' separated. In the last scenario the entanglement between a, b'' and c'', d is preserved and photons a, d remain in a product state. In any case Alice and Bob do not know whether their photons got entangled or not after they have already been measured. That's what Victor has to tell them afterwards.

In a paper by C. Brukner et al. [5], it is also shown that by tuning the phase from $0 \le \varphi \le \frac{\pi}{2}$ one can observe a complementarity relation between the degree of entanglement of photons a, b'' and c'', d on one side and the purity of entanglement for pairs a, d and

b'', c'' on the other.

Peres supposed that: *[...]"if we attempt to attribute an objective meaning to the quantum state of a single system, curious paradoxes appear: quantum effects mimic not only instantaneous action-at-a-distance but also, as seen here, influence of future actions on past events, even after these events have already irrevocably recorded."* [4]

3. Generation of Entangled Photon Pairs

There are many ways how one can create entangled photon pairs e.g. in waveguides [30, 31], in a Sagnac Loop Interferometer [32, 33] or for example in a optical cavity [34]. In our experiments we produced entangled photon pairs by Type-II spontaneous parametric down-conversion (SPDC). A high intensity femto-second Laser hits a birefringent, non centro-symmetric crystal with nonlinear electric susceptibility. There the pump photon has a small probability to spontaneously decay into two photons. In this process energy and momentum has to be preserved:

$$\hbar\omega_p = \hbar\omega_1 + \hbar\omega_2$$
$$\hbar\vec{k}_p = \hbar\vec{k}_1 + \hbar\vec{k}_2$$

(3.1)

Here ω_p denotes the frequency of the pump photon whereas $\omega_{1,2}$ symbolizes the frequency for the decayed photons 1 and 2. $\vec{k}$ represents the wave vector inside the crystal.

The photons of a wavelength are emitted on cones (see figure 3.1) determined by the phase-matching condition. The direction of a single photon on one of these cones is completely random, but when one photon is detected, the presents of its twin on the other cone is heralded. Type-II parametric down-conversion means that they have opposite polarization. The optical axis of the down-conversion crystal with respect to the pump beam can be adjusted for a collinear-emission (the two rings are overlapping on only one point, the center of the pump beam) or for a non-collinear emission (every other scenario). In our experiments we used the advantages of both types.

This physical phenomenon of frequency conversion occurs in many different crystals (BBO, KTP, KDP,...) and can be used to create different types of entangled photon pairs i.e. polarization-entangled [35], momentum-entangled [36] and time-entangled [37]. A more detailed description about the production of entangled photon pairs and the different types of entanglement can be found in various books and papers e.g [38, 39].

3.1. Non-collinear Photon Pair Source

For the generation of polarization-entangled photon pairs, a non-collinear emission is very common. The emission angle of the ordinary (o-beam) and extraordinary beam (e-beam) can be adjusted by the cutting angle i.e. the angle between the pump beam and the optical
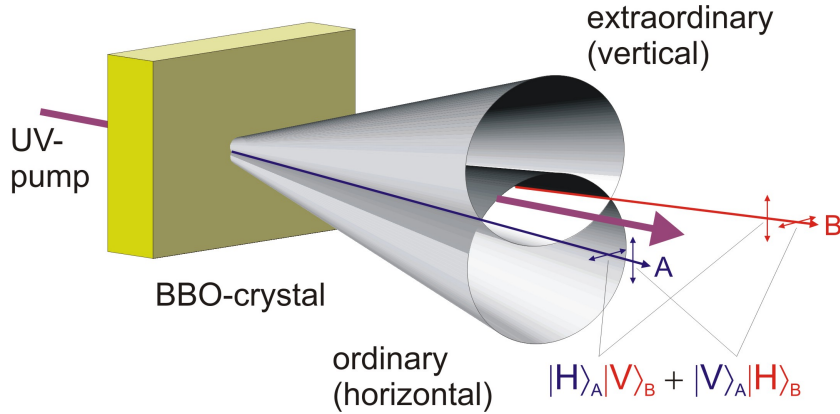
Figure 3.1.: *A schematic picture of Type-II spontaneous parametric down-conversion taken from [20]. The two photons emerge on cones called ordinary (horizontal polarized) and extraordinary (vertical). The emission angle is governed by the phase-matching condition. On the intersection point the photons carry no information about where they emerged from, but their polarization will be opposite.*

axis of the crystal. At the intersection lines of the two cones, one cannot tell whether a photon emerged from the e-beam or the o-beam if the walk-off effects are compensated correctly (see next chapter 3.1.1). Thus it is impossible to know if a photon is H or V polarized and therefore the state of these two intersection lines is in a superposition of $|H\rangle|V\rangle$ and $|V\rangle|H\rangle$ and can be written as

$$|\Psi\rangle = \frac{1}{\sqrt{2}}(|H\rangle_1|V\rangle_2 + e^{i\alpha}|V\rangle_1|H\rangle_2) \qquad (3.2)$$

Due to the birefringence of the crystals the photons get an additional phase which is taken into account by the value α (see figure 3.1). This phase can be tuned by tilting one of the compensation crystals, from 0 to π (see figure 3.2). The compensation crystals will be explained in the next chapter. By flipping the polarization by 90° in one arm (for example with a half-wave plate) and adjusting the phase properly one can create all of the four Bell-States:

$$|\Psi^\pm\rangle = \frac{1}{\sqrt{2}}(|H\rangle_1|V\rangle_2 \pm |V\rangle_1|H\rangle_2)$$
$$|\Phi^\pm\rangle = \frac{1}{\sqrt{2}}(|H\rangle_1|H\rangle_2 \pm |V\rangle_1|V\rangle_2) \qquad (3.3)$$

This source for polarization-entangled photon pairs was introduced by Paul G. Kwiat et al. in 1995 [35].

3.1.1. Compensation of the birefringent Walk-Off Effects

Since we are using a birefringent BBO crystal ($\beta - Barium - Borate$), we have to compensate two walk-off effects. The transversal walk-off effect leads to a spatial shift of the two cones whereas the longitudinal or timing walk-off would in principle give you some information about where the photon was emitted. Both effects can be compensated by using two half-wave plates (HWP) and additional BBO crystals before each fiber coupler (see figure 3.2). The compensation crystals have half the thickness of the original crystal and their optical axis is oriented along the same angle. The HWP rotates the polarization by 90° and therefore exchanges ordinary and extraordinary beam. Now the exchanged photons pass trough the compensation crystal where they experience the same effects. In this way the longitudinal walk-off gets erased and the transversal is at least reduced. A more detailed description of this kind of source and the compensation of walk-off effects can be found in [40, 41].
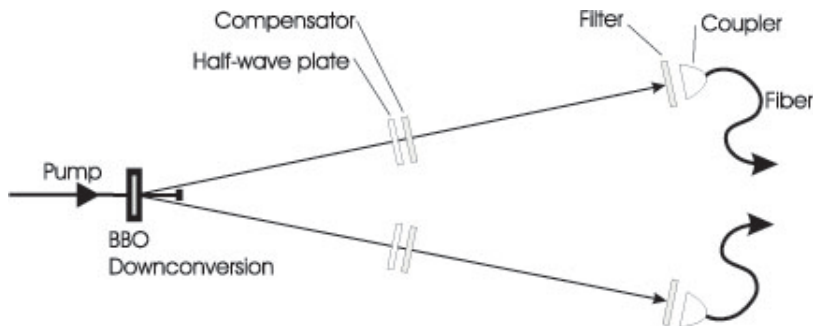

Figure 3.2.: *A schematic source for polarization-entangled photon pairs. The half-wave plate and the second BBO (Compensator) compensate the walk-off effects that occur in the first down-conversion crystal. The interference filter and the single-mode fibers provide better spatial filtering and increase the entanglement visibility. Picture taken from [27].*

3.1.2. Experimental Realization of the SPDC Source

A picture of the real setup can be seen in figure 3.3. A *Chameleon Laser System* from the company *Coherent GmbH* produces femto-second laser pulses at 808 nm with 7 nm full width at half maximum (FWHM). The repetition rate is 80 MHz and the Ti:Sapphire crystal has an average output power of 4 W. The infrared beam is focused into a second harmonic generation crystal (SHG) where a strong UV pulse at 404 nm is created. Our SHG crystal is also a BBO (0,7 mm thickness, cut for Type-I phasematching[1]). The maximum achieved UV power was 1,6 W. Afterwards the beam has to pass several UV

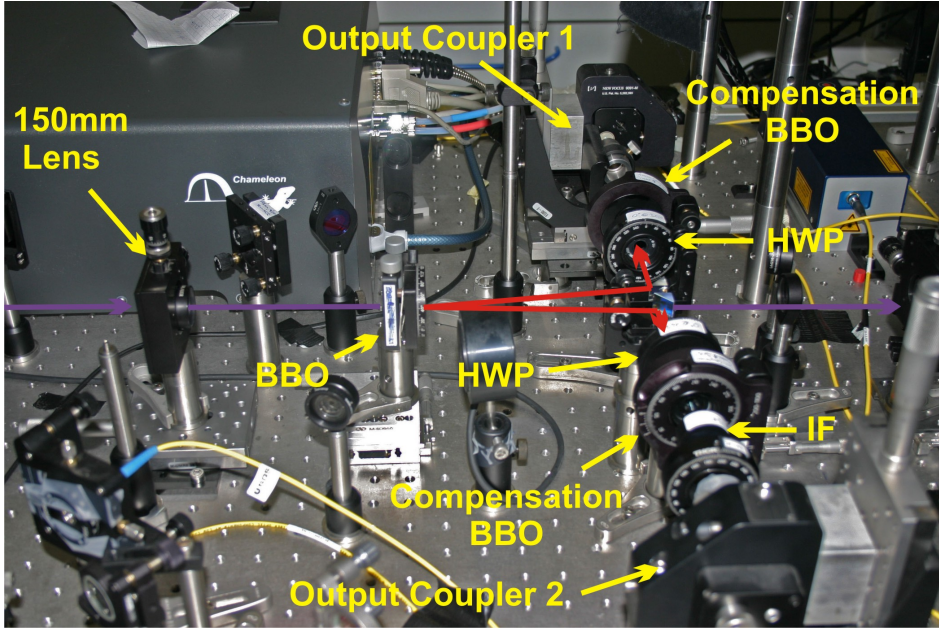[1]Type-I means that the two emitted photons have identical polarization.

Figure 3.3.: *A picture of our non-collinear setup for polarization-entangled photons. A strong UV pulse at 404 nm (purple line) is focused with a 150 mm lens into a down-conversion crystal (BBO). The walk-off effects between the emitted photon pair (red lines) is compensated by a half-wave plate (HWP) and a compensation crystal. The narrow-band interference filter (IF) and the single-mode fibers (Output Coupler) guarantee good spectral and spatial filtering. For details see text.*

mirrors before it reaches the down-conversion crystal. Those mirrors are highly reflective for UV (reflectivity at 370-425 nm $\geq 99,8\%$) and highly transparent for infrared (reflectivity at 800 nm $\leq 2\%$). The reason for doing this is to guarantee that no infrared light propagates through our setup and creates a background signal.

The UV pulses are focused with a 150 mm lens into the down-conversion crystal (BBO Type-II, 2 mm, $\Theta = 43,5$). The down-converted 808 nm photons hit a high reflective prism before they pass the compensation unit. After the narrow-band interference filter they are coupled into anti-reflection coated (AR) single-mode fibers. The narrow-band filters guarantee spectral filtering and the single-mode fibers asure a good spatial filtering. In this way a higher entanglement visibility can be achieved.

Since we need two entangled photon pairs for the delayed-choice entanglement swapping experiment, we recycle the UV pump by focusing into another BBO. The second source contains of the same components as the first one.

The highest count rates we were able to achieve in our two sources at the maximum UV power of 1,6 W were:

- Source 1: 310.000 coincidences with 2.4 and 2.7 mio singles. The entanglement

contrast for a $|\Psi^-\rangle$ state was usually between 5:1 and 6:1 for both bases (H/V and +/-), which corresponds to a visibility of $67\% - 70\%$.

- Source 2: 165.000 coincidences with 2 and 2.3 mio singles. The visibility is the same as for the first source.

The source visibility is so low, because of the higher-order emission. With this high UV pump power of 1,6 W the crystal has an increased possibility to emit two or even three photon pairs instead of one. Therefore the probability to detect two uncorrelated photons is higher than with a lower pump power.

3.2. Collinear Photon Pair Source

The two "crossed rings" down-conversion setups for polarization-entanglement will be used for the delayed-choice entanglement swapping experiment. In all the other experiments described in this thesis, we used another type of source. In a collinear setup, ordinary and extraordinary beam are overlapping on just one point (the center of the pump beam) and therefore the photon pair is emitted into the same spatial mode. Like in the non-collinear down-conversion scheme, the emitted photons are entangled in energy (because of the energy conservation each down-conversion photon has half the frequency of the pump photon) and time (both photons are emitted at the same time). Therefore by detecting one photon, the presents of its twin is heralded. Since this is a Type-II SPDC process the photons have opposite polarization.

For this kind of source we also use a 2 mm BBO ($\Theta = 43, 5$), but this time the tilting is optimized for collinear emission. The UV pump is focused into the crystal and coupled out afterwards with a high-reflective UV mirror (see figure 3.4 and figure 3.5). A broadband interference filter separates the rest of the UV pump from the down-converted photons. The photon pair is split on a PBS and coupled into single-mode fibers for further process. We have chosen this type of source to test the performance of our switchable beam splitter, because it is more stable and easier to adjust than the non-collinear one.
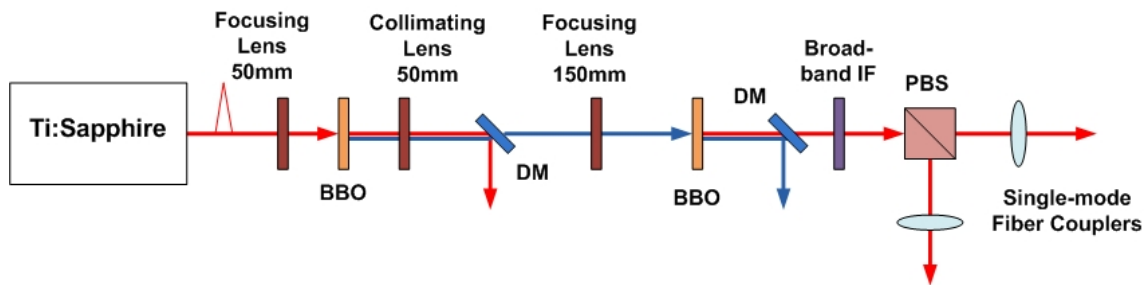
Figure 3.4.: *A schematic picture from our collinear down-conversion setup. A Ti:Sapphire Laser produces infrared pulses which are up-converted in a SHG unit. For higher efficiency we focus the infrared beam with a 50 mm lens into the BBO crystal. Afterwards the infrared light is coupled out via a dichroic mirror (DM, highly transparent for UV and highly reflective for infrared). The UV pump is focused into a 2 mm BBO and is coupled out by another dichroic mirror (this time highly reflective for UV and transparent for infrared). The broadband interference filter (IF) blocks the rest of the UV light. The down-converted photon pairs are emitted into the same spatial mode and have opposite polarization (H and V). They are separated on a polarizing beam splitter (PBS) and coupled into single-mode fibers.*
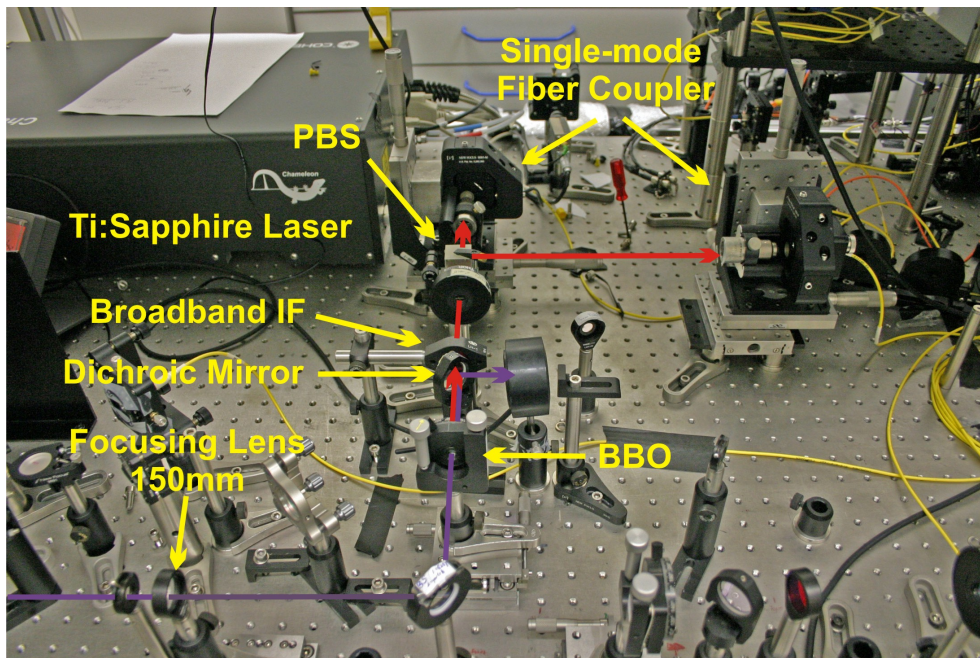

Figure 3.5.: *A picture of our collinear SPDC setup. For a detailed description see text and figure 3.4.*

4. Interferometric Switchable Beam Splitter

Our main goal is to perform a delayed-choice entanglement swapping experiment as described in chapter 2.7. For this we need a fast switchable Bell-state analyzer. Since the realization of such a device is not easy and because it consists of many components which must be optimized and tested separately, I will describe every crucial building step and test measurements that we performed, very carefully. The next two chapters describe experiments which were done to check if our setup fullfils the high requirements needed for the realization of a delayed-choice entanglement swapping experiment.

The development of this fast tunable interferometric switchable beam splitter (TBS) is an extension of the work by my colleague Nuray Tetik [42]. Parts of her diploma thesis show in a proof-of-principle experiment that a setup as shown in figure 4.1 can work as a fast switchable beam splitter, which will be used in the delayed-choice entanglement swapping experiment. We extended her setup in many ways. First of all, we had to care more about the stability of the setup than she did. Every interferometer is sensitive to all kinds of mechanical vibrations and even acoustic noise. Therefore we exchanged every mount with ultrastable posts and designed the interferometer more compactly in order to build an isolation box around it. We also installed new Pockels Cells with a higher repetion rate of up to 5 MHz instead of 800 KHz. In my experiments we used single and entangled photons and therefore we had to install single-mode fiber couplers to guide the output photons to Avalanche Photo Diodes (APDs). We also increased the efficiency by exchanging every optical component (mirrors, beam splitters etc.). In the old setup, those elements were optimized for $\lambda = 710$ nm wavelength. Our laser emits femto second pulses at $\lambda = 808$ nm and if we had used the old setup in combination with our laser, we would have suffered from severe losses on every optical component. Another important difference is, that we installed additional BBO crystals in each arm of the Mach-Zehnder interferometer. Those BBO crystals compensate some unknown birefringence, which occured in the setup and limited the interference visibility for $\pm 45°$ polarized light.

4.1. Mach-Zehnder Interferometer

To realize a polarization-independent fast switchable beam splitter we used a Mach-Zehnder interferometer with one Pockels Cell (or electro-optical modulator (EOM)) in each arm as sketched in figure 4.1. The theory below shows that by tuning the phase with the Pockels Cells inside the interferometer one can control the splitting ratio of this beam splitter. An arbitrarily polarized photon state in input mode a can be described as

$$|\Phi\rangle = (\alpha|+\rangle + \beta|-\rangle)\,|a\rangle \tag{4.1}$$

Here $|+\rangle$ ($|-\rangle$) stands for a $+45°$ ($-45°$) photon and $|\alpha|^2 + |\beta|^2 = 1$.

The reason why we use this basis for our calculation is that the optical axis of the crystals inside the Pockels Cells is aligned at $+/-$ but this will be explained later. A non-polarizing
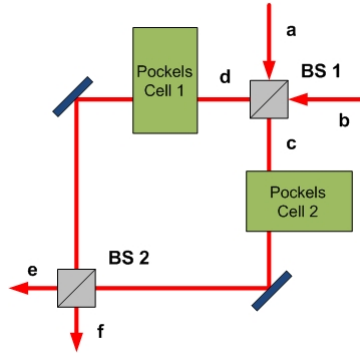

Figure 4.1.: *A schematic figure of tunable beam splitter. It consist of a Mach-Zehnder interferometer with one Pockels Cells in each arm. The Pockels Cells apply a voltage dependent phase shift on each arm. The calculations show that by tuning the phase from 0 to π one can set the splitting ratio on BS2 to an arbitrary ratio.*

symmetric beam splitter acting on a photon in input mode a can be described by

$$|a\rangle \rightarrow \frac{1}{\sqrt{2}}|c\rangle + \frac{1}{\sqrt{2}}i|d\rangle \tag{4.2}$$

That means that after the first beam splitter the state $|\Phi\rangle$ evolves to[1]

$$|\Phi\rangle = \frac{1}{\sqrt{2}}((\alpha|+\rangle + \beta|-\rangle)\,(|c\rangle + i|d\rangle) \tag{4.3}$$

As one can see in figure 4.1 Pockels Cell 1 is only acting on spatial mode d and Pockels Cell 2 on spatial mode c. I assume that the optical axis of EOM 1 is aligned at $|+\rangle$ and EOM 2 at $|-\rangle$. Therefore Pockels Cell 1 gives a phase shift $\varphi(V_1)$ on $+45°$ polarized light and no

---

[1]In this calculation I set the phase within the interferometer to 0 and ignore the phase changes on mirrors.

phase shift on -45°. Pockels Cell 2 gives a phase shift $\varphi(V_2)$ on -45° and no shift on +45°. V_i stands for the applied voltage. For simplicity let's assume that $\varphi(V_1) = \varphi(V)_2 = \varphi(V)$. This assumption stands as long as the EOMs are well aligned and if the applied voltage is the same for each crystal.

After the Pockels Cells the input state evolves to

$$|\Phi\rangle = \frac{1}{\sqrt{2}} \left(\alpha \exp^{i\varphi(V)} |+\rangle|c\rangle + i\alpha|+\rangle|d\rangle + \beta|-\rangle|c\rangle + i\beta \exp^{i\varphi(V)} |-\rangle|d\rangle \right) \qquad (4.4)$$

The second beam splitter recombines the two paths and the state becomes

$$|\Phi\rangle = \frac{1}{2} \left[\left(1 - \exp^{i\varphi(V)} \right) (\alpha|+\rangle - \beta|-\rangle) |e\rangle + i \left(1 + \exp^{i\varphi(V)} \right) (\alpha|+\rangle + \beta|-\rangle) |f\rangle \right] \quad (4.5)$$

Now that we know our final state we can think about special cases depending on the value of φ.

- $\varphi(V) = 0$

  Both Pockel Cells are OFF (applied voltage is 0). It's easy to see that the left hand term vanishes and only the second term survives. The output state is

  $$|\Phi\rangle = i \left(\alpha|+\rangle + \beta|-\rangle \right) |f\rangle \qquad (4.6)$$

  and therefore equals the input state 4.1. A photon entering in spatial mode a will always exit in mode f with its polarization state preserved.

- $\varphi(V) = \frac{\pi}{2}$

  Both Pockels Cells are ON and apply a $\frac{\pi}{2}$-voltage to the crystals. The output state looks like

  $$|\Phi\rangle = \frac{1}{2}(1-i)[(\alpha|+\rangle - \beta|-\rangle) |e\rangle - (i-1)(\alpha|+\rangle + \beta|-\rangle)|f\rangle] \qquad (4.7)$$

  One can see from this result that the photon has equal probability to exit in spatial mode e or f. It is important to note that the polarization of a photon which ends up in mode e (gets reflected on the second beam splitter) is not preserved. Due to the minus sign before the $|-\rangle$ part this component of the polarization is rotated by 90°. For instance a -45° input that gets reflected on beam splitter 2 is rotated to +45°.

- $\varphi(V) = \pi$

  Both Pockels Cells are ON and apply a π-voltage to the crystals. In this case the right hand therm of equation 4.5 vanishes and the output is

  $$|\Phi\rangle = (\alpha|+\rangle - \beta|-\rangle) |e\rangle \qquad (4.8)$$

Hereby the photons will always end up in mode e and their $|-\rangle$ polarization component is rotated by 90°.

To be consistent I will also write down the final state for a photon entering the interferometer in spatial mode b.

$$|\Phi\rangle = \frac{1}{2}\left[i\left(1 + \exp^{i\varphi(V)}\right)(\alpha|+\rangle + \beta|-\rangle)|e\rangle + \left(1 - \exp^{i\varphi(V)}\right)(\alpha|+\rangle - \beta|-\rangle)|f\rangle\right] \quad (4.9)$$

And in the three cases discussed above it evolves as follows

- $\varphi(V) = 0$: $|\Phi\rangle = i\left(\alpha|+\rangle + \beta|-\rangle\right)|e\rangle$

- $\varphi(V) = \frac{\pi}{2}$: $|\Phi\rangle = \frac{1}{2}(1-i)[(\alpha|+\rangle + \beta|-\rangle)|e\rangle + (1-i)(\alpha|+\rangle - \beta|-\rangle)|f\rangle]$

- $\varphi(V) = \pi$: $|\Phi\rangle = -\left(\alpha|+\rangle - \beta|-\rangle\right)|e\rangle$

This result is equivalent to the first one, only the output modes are different.

Conclusion

We conclude that a Mach-Zehnder interferometer with one Pockels Cell in each arm can work as a fast switchable beam splitter. By switching the applied voltage on the crystals between 0 and $\frac{\pi}{2}$ one can decide to use the beam splitter or not to use it. According to what we will show in section 4.2.4 this decision can be done very fast.

4.2. Experimental Setup

The Mach-Zehnder interferometer shown in figure 4.1 is only an idealization. The actual setup looks more like in figure 4.2 and in figure 4.3. In this section I will carefully explain every detail of the experimental setup.

4.2.1. Performance of the Mach-Zehnder

A good interference visibility is essential for every experiment we are going to perform with our tunable beam splitter (TBS). Here I want to explain how we aligned the Mach-Zehnder interferometer and present some results which show its good performance.

When we started to build this setup we decided not to use only two mirrors to recombine the two beams. Instead we used a combination of one prism and two high reflective mirrors on a translation stage in each arm. There are two good reasons for doing that.

First of all it is much easier to overlap the two beams on the second beam splitter because one has more degrees of freedom. Secondly every Mach Zehnder interferometer is sensitive to the coherence length of the input laser. The two arms must have exactly
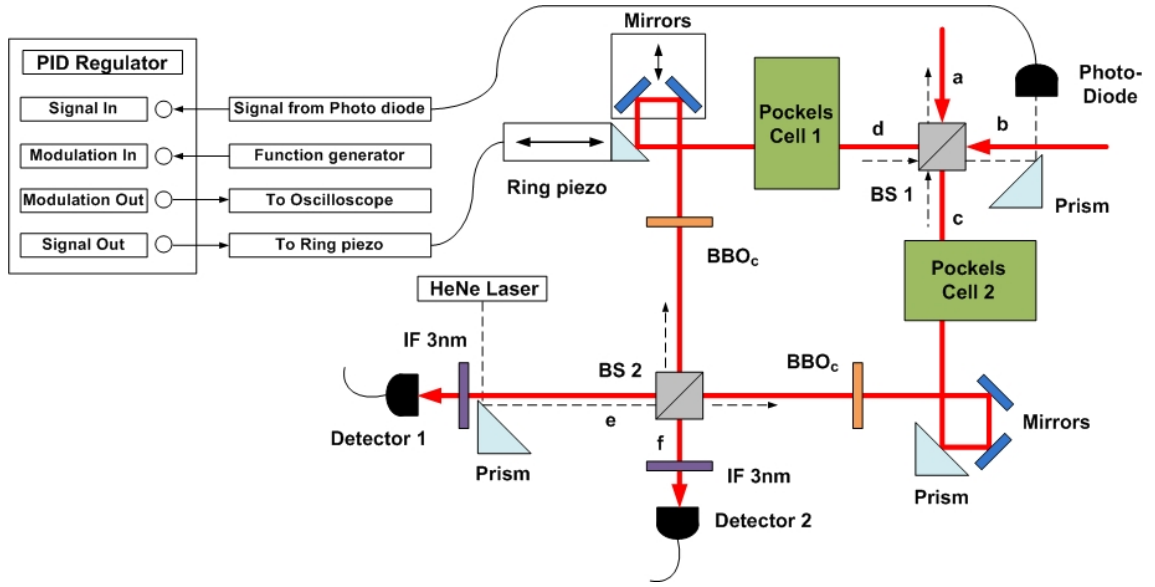
Figure 4.2.: *Illustration of the experimental setup. One Pockels Cell is placed in each arm of Mach-Zehnder interferometer, which vary the phase of the incoming beam. The output modes are coupled into single-mode fibers and guided to APD detectors. Additionally we use 3 nm interference filters (IF) in modes e and f for better spectral filtering. Two BBO crystals (BBOc) compensate some unknown birefringence, which limited the visibility in +/- basis. To actively stabilize the interferometer (see chapter 4.2.2), we use a HeNe Laser which counter-propagates through the setup and produces a reference signal on a photo diode. This signal is analyzed by a PID regulator, which controls a ring piezo inside the interferometer. For a more detailed description see text.*

the same length otherwise the visibility will decrease and even vanish when the difference gets too large. There is only a certain path length difference where you will still see some interference but this is strongly depending on the coherence length of the laser. For our femto second laser this is only a few micrometers. Therefore we mounted the two mirrors on a motorized translation stage in order to change the length of one arm very accurately. With this trick one can systematically search for the region where the two arms of the interferometer have no path length difference.

We did that by attenuating our laser down to the single-photon level with neutral density filters and guided them over single-mode fibers into the interferometer. Output modes e and f are also coupled into single-mode fibers and plugged into commercial single-photon detectors. If the two beams are spatially overlapping on the second beam splitter and the longitudinal difference is within the coherence length of the laser you can see interference between the two output modes. If one of this two criteria is not satisfied you will not see any interference.

The transversal overlap was found by looking at the two beams directly after the last
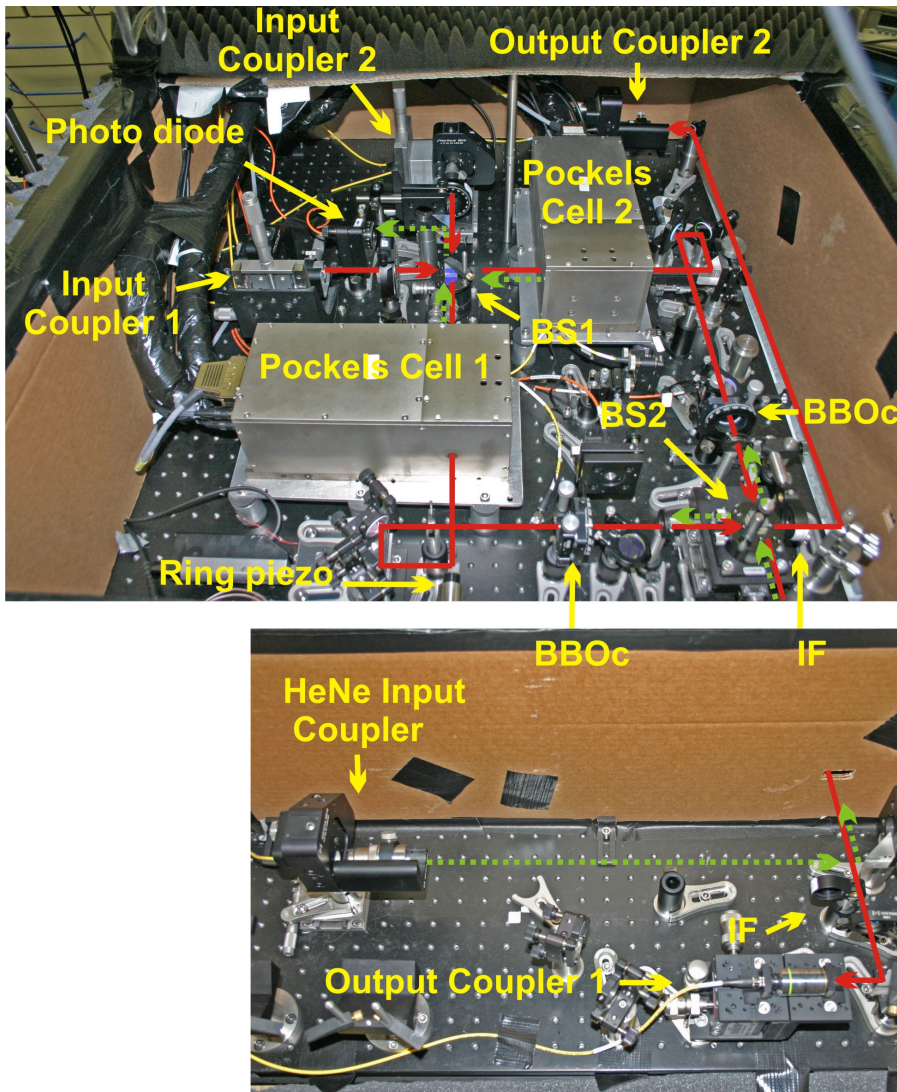
Figure 4.3.: *Pictures of the interferometrical switchable beam splitter setup. It consist of a Mach-Zehnder interferometer (realized by two beam splitters (BS1 and BS2) and several mirrors (not labeled)) and one Pockels Cell in each arm. Two BBO crystals (BBOc) compensate some unknown birefringence. On the input and output couplers we use single-mode fibers for better spatial filtering. The 3nm interference filters (IF) guarantee good spectral filtering. To actively stabilize the Mach-Zehnder (for more details see chapter 4.2.2) we installed a HeNe Laser which counter propagates through the setup (dashed green line) and is detected by a photo diode. This reference signal is send to a PID regulator which controls a ring piezo inside the interferometer. Additionaly to that we encloused the setup in a box to maximize the passive stabilization. For more details see text.*

beam splitter. There the overlap can be achieved by tilting the two mirrors in each arm. Then one has to look at the two spots far away from the the first observation point to guarantee that they are not diverging. The overlap in this region is mostly influenced by the tilting of the last beam splitter. After this was done we started to scan the correct path length difference.

The results of such a scan measurement can be seen in figure 4.4. The width of this interference bubble corresponds to the coherence length of the input laser. In the interference region, the single photon count rate varies strongly depending on the position of the motorized stage.
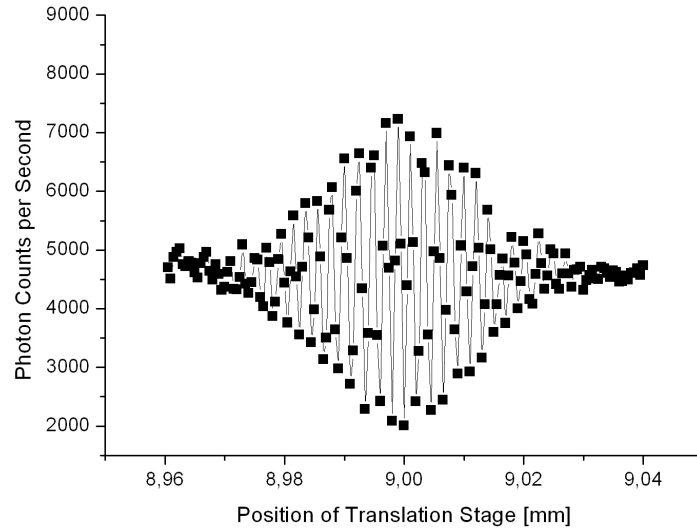

Figure 4.4.: *The result of a measurement to find the correct path length difference between the two arms of the Mach-Zehnder interferometer. It shows the single photon count rate of detector 1 plotted against the position of the motorized stage where the two mirrors are mounted (see figure 4.2). If the path length difference is within the coherence length of the input laser, single photon interference shows up. This measurement was performed with our pulsed infrared laser which was attenuated to single photon level with neutral density filters.*

The two outputs of the Mach-Zehnder behave opposite. If the count rate of detector 1 is rising, the one of detector 2 is falling and vice versa. This can be explained in the following way:

Whether a photon exits in mode e or f depends on its phase. As we know from the equations in section 4.1, light coming from input a will always be registered by detector 2, if the phase shift applied by the Pockels Cells is 0 or 2π. If the phase difference equals to π one will always find the photons in mode e.

Now it is important to know that a phase shift can not only be applied by the EOMs. In principle every component gives an additional phase to the beam, for example the reflection on a mirror. But if the interferometer is aligned well most of it is canceled out since the drifts are the same for both arms c and d. In our measurement we have a situation where two mirrors are constantly moving and therefore the phase of the input beam varies with the position of the translation stage.
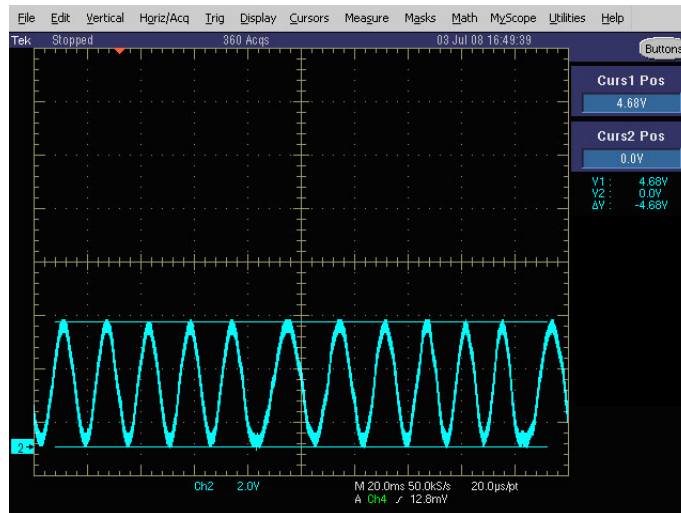

Figure 4.5.: *Interference fringes from detector 1 produced by a 808 nm input from our pulsed infrared laser system. The x-axis corresponds to the phase which is modulated by the slowly moving ring piezo. The phase variation is monitored over time (in this case 20 ms/div). The y-axis represents the intensity measured in voltage which is registered at the photo diode (2 V/div). We measure the minimum and maximum position with two cursors. From the measurement results which can be seen on the right, we are able to calculate the interference visibility.*

Once the correct path length difference is found one can use a faster method to reveal the interference. By constantly moving one prism forwards and backwards one can also apply a periodic phase change. We mounted one of the prisms on a ring piezo and applied a slow ramp-signal to it coming from a function generator (see figure 4.2). Instead of single photons we used a strong laser beam inside the interferometer which can easily be detected with normal photo diodes. Those diodes produce an electronic signal proportional to the intensity of the incoming light. We measured this signal on an oscilloscope. The results of such a measurement can be seen in figure 4.5. From those pictures we are able to calculate the visibility which gives you a quantitative value to characterize your interference. It is calculated in the following way:

$$V = \frac{I_{max} - I_{min}}{I_{max} + I_{min}} \tag{4.10}$$

I_{max} is the maximal recorded intensity while I_{min} is the minimum. It is obvious that

100% visibility coresponds to perfect interference while 0% means that the two beams are not interfering at all and have the same value. In that way we could easily optimize our Mach-Zehnder by adjusting the transversal and longitudinal overlap on BS2, because every adjustment influenced the visibility and was instantaneously recorded on the oscilloscope.

The interferometer was optimized until the visibility was $98 \pm 2\%$ for input mode a and every input polarization (Vertical, Horizontal, +45°, -45°). The polarization was adjusted with a polarizer before beam splitter 1 (not shown in figure 4.2). The alignement of the second input mode b is a bit more crucial and will be described in chapter 4.2.3.

When we started to set the interferometer up, we noticed that the visibility in +/- basis was much lower (approximately 60%) than for H or V. Therefore we placed two BBO crystals (called BBOc in figure 4.2) in each arm of the Mach-Zehnder to compensate some unknown birefringence. This method worked out very well and finally the interference quality is very high in every polarization basis.

4.2.2. Stabilization and Phase-locking

For our experiments it was very important to stabilize the phase of the interferometer. Therefore we produced a reference signal with a HeNe laser ($\lambda = 632$ nm) which was coupled backwards through the setup as you can see in figure 4.2. A PID regulator compensated errors between this signal and a desired setpoint by controlling the ring piezo inside the interferometer (PID stand for Proportional Integral and Differential and the reaction of the regulator can be tuned by those three parameters). The setpoint was adjusted to the middle of the fringes because there the locking showed the highest stability[2].

By using this PID regulation loop we achieved two things:

- Noise caused by mechanical vibrations was compensated for the reference and therefore also for the main signal. In this way we could actively stabilize our interferometer.

- We were also able to lock the phase of the interferometer to a certain position, e.g. where all the photons exit in one mode or where both outputs are balanced.

The active stabilization worked well but it was not possible to compensate every disturbance. In figure 4.6 one can see the error signal from the PID output while I was slightly knocking on the optical table.

That shows how easy it was to disturb the phase locking of the interferometer. Therefore we decided to maximize the passive stabilization in the following way:

- First of all we mounted every optical component on 1 inch pillar posts. They have a fixed height and provide higher stability than normal mounts.

---

[2]The visibility of our reference signal is about 80% which is enough to achieve a good phase locking effect
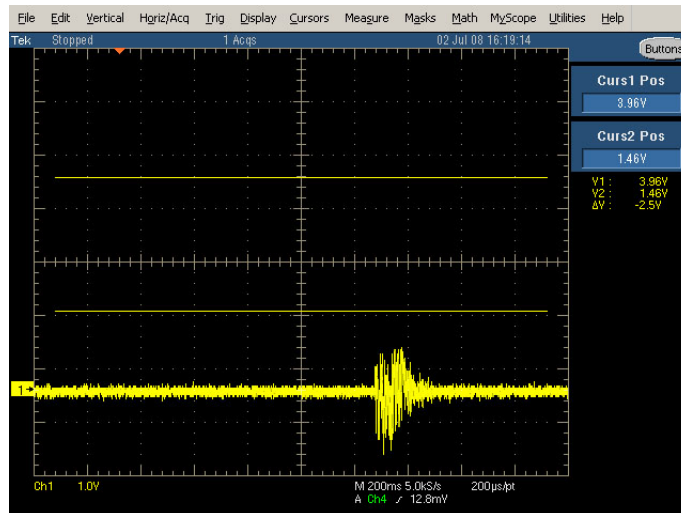
Figure 4.6.: *Error signal from the PID feedback loop. It is the difference between the set-position and the current position. Ideally it should be zero all the time. The spike in the middle shows the fast disturbance while I was slightly knocking on the optical table. The phase locking is interrupted for more than 200 ms. This picture shows how important it is to protect the interferometer from mechanical vibrations and ambient noise. The x- and y-axis is given in units of 200 ms/div and 1 V/div.*

- The Pockels Cells are cooled with a internal fan and with a water cooling system. In order to damp those mechanical vibrations we put rubber underneath the driver box. This trick was first tested by Nuray Tetik [42].

- Additionally we built a box around the whole setup and glued some noise damping material on it. This box protects the interferometer from acoustic noise and holds of the air flow from our air condition. It also guarantees that no ambient light disturbs our measurements.

4.2.3. Alignment of the Second MZI Input Mode

The previous results show only the performance of the first input coupler (mode a see figure 4.2). But for the aimed delayed-choice entanglement swapping experiment (see chapter 6) we need to use the second MZI input mode b. For the success of this experiment it is necessary that the two inputs of the interferometric switchable beam splitter have a high visibility and are spatially overlapping well.

The alignment of the second mode was more difficult than the first one. In order to keep the alignment of the interferometer for input mode a, we had to avoid touching anything except the input coupler in mode b because otherwise we would have misaligned input a. But since we used single-mode fibers on the input and output couplers we achieved that

with a nice trick.

We guided a strong laser beam (several mW) to input a and measured the output power in the single-mode fibers at the two outputs of the Mach-Zehnder. Then we applied the same intensity to the second mode b and aligned the input coupler until the power in the output fibers was the same as for the first one. Afterwards we observed the visibility for the second input mode b on the oscilloscope and optimized it until it was as good as for the first input mode a.

This trick worked out well because our single-mode fibers have a core diameter of approximately $5\mu m$. Therefore the spatial overlapping of mode a and b is automatically fulfilled if the input and output power in the single-mode fibers is the same for both inputs.

To verify that both input modes were spatially overlapping we used the following method[3]: We split the light from our laser on a fiber beam splitter and guided them to our two input couplers. If both modes are well overlapping in the Mach-Zehnder and if the intensity coming from each input is balanced one should not be able to observe any interference on the oscilloscope. One will only see a flat line at the maximum of the fringes.

The reason for this is clear. The amplitudes of the two incoherent input beams in mode a and b are always summed up to 1 at the output modes. Imagine that the phase shift inside the interferometer is 0 or π. As we know from the calculations in chapter 4.1 a photon entering in mode a (b) will always exit in mode f (e). When the phase changes from 0 to $\frac{\pi}{2}$ the probability for detector 2 to register a photon coming from mode a (b) changes from $p = 1$ ($p = 0$) to $p = 0.5$ ($p = 0.5$). Therefore the summarized probability for a detector to see a photon is always $p = 1$, independent from the phase.

The figures 4.7 show the interference pattern from input a and b while the other one was blocked. In the lower figure both modes are unblocked and therefore the fringes cancel each other. The reason why one can still see some residual interference pattern is that the mode overlap was not perfect and because the amplitudes of both input beams was slightly different.

4.2.4. Pockels Cells

Since the Pockels Cells are a very crucial building block of our tunable beam splitter, I want to characterize them more carefully in this chapter. First I want to introduce the theory behind electro-optical modulators (EOMs) and then describe their operation mode and performance.

Certain anisotropic piezoelectric crystals change their refractive index when subjected to an electric field. If this modification is proportional to the applied electric field, it is called

---

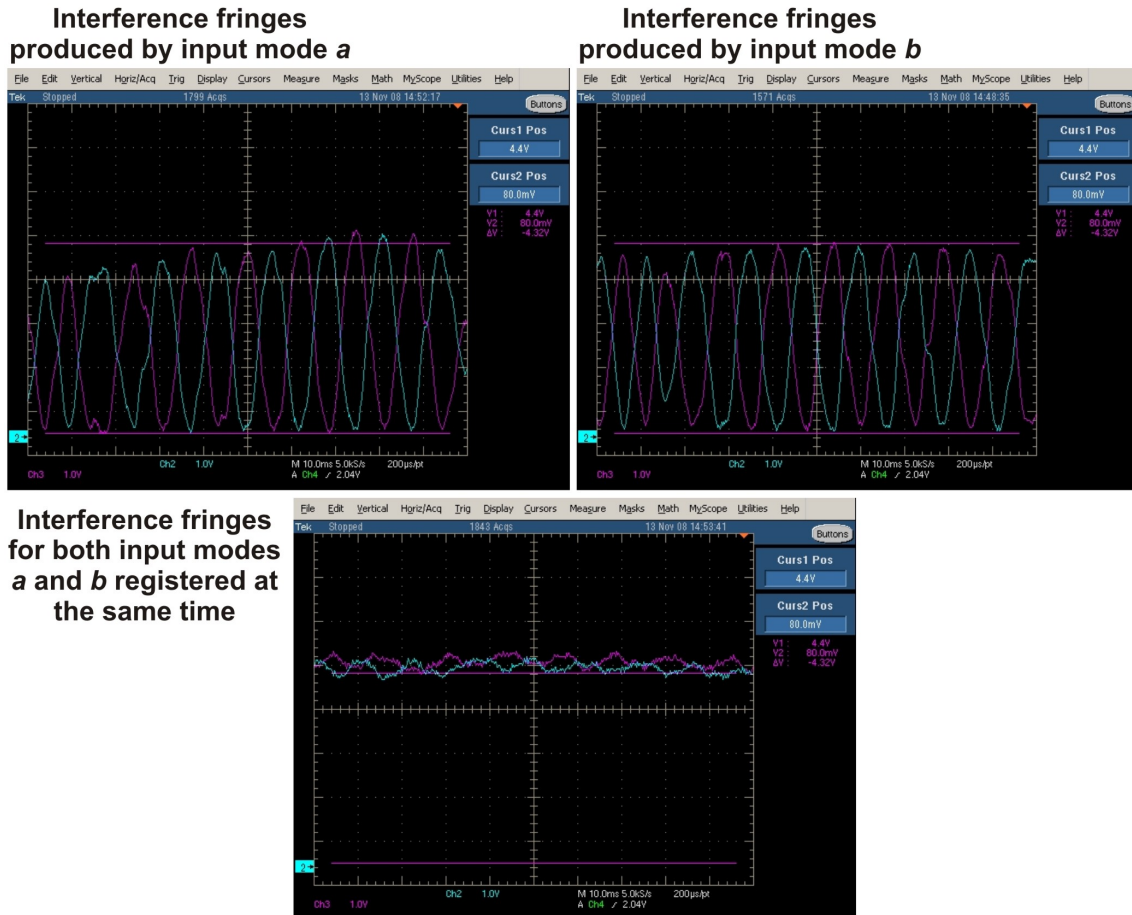[3]One could also measure a two-photon interference (HOM) but this will be explained later (see chapter 5.1)

Figure 4.7.: *The upper two figures show the interference fringes for input a and b separately. The x-axis corresponds to the phase which is modulated by the slowly moving ring piezo. The phase variation is monitored over time (in this case 10 ms/div). The y-axis represents the intensity measured in voltage which is registered at the photo diode (1 V/div). The amplitude drifts are due to fluctuations in the laser output power. If both incoherent input modes are overlapping well inside the Mach-Zehnder and if they have the same amplitude, both interference fringes are summed up and therefore no interference pattern is observed (see lower picture). The reason why we can still see residual interference is that the mode overlapping was not perfect and mainly because the amplitudes of both input beams were sightly different.*

Pockels Effect or linear electro-optical effect[4]. This was discovered by Friedrich Pockels in 1893 [43]. In the Taylor series expansion the refractive index can be written as follows [44]

$$n(E) = n(0) + \frac{dn}{dE}E + \frac{1}{2}\frac{d^2n}{dE^2}E^2 + ... \tag{4.11}$$

It is convenient to rewrite this equation in terms of $r = -\frac{2}{n^3}\frac{dn}{dE}$ and $s = -\frac{1}{n^3}\frac{d^2n}{dE^2}$ which are know as the electro-optic coefficients.

$$n(E) = n(0) - \frac{1}{2}rn^3E - \frac{1}{2}sn^3E^2 - ... \tag{4.12}$$

For Pockels Cells the third term from equation 4.12 can be neglected.

Electro-optical crystals have many applications these days. Here I only want to explain those which are important for our experiments.

Pockels Cells as Dynamic Wave Retarders

Let's assume that our wave travels parallel along the z-axis through the crystal. If an electric field is applied the refractive index in the x- and y-axis changes in the following way [44]:

$$n_x(E) = n_x(0) - \frac{1}{2}r_x n_x^3 E \tag{4.13}$$

$$n_y(E) = n_y(0) - \frac{1}{2}r_y n_y^3 E \tag{4.14}$$

Therefore the two polarization modes of our beam travel with different velocities. After the distance L (length of the crystal) the phase retardation between the two modes[5] becomes

$$\Phi = \frac{2\pi}{\lambda}(n_x(E) - n_y(E))L = \frac{2\pi}{\lambda}(n_x(0) - n_y(0))L - \frac{\pi}{\lambda}(r_x n_x^3 - r_y n_y^3)LE \tag{4.15}$$

If the voltage V is applied between the surfaces of the crystal separated by the distance d, we can rewrite equation 4.15 as [44]

$$\Phi = \Phi_0 - \pi\frac{V}{V_\pi} \tag{4.16}$$

were

$$V_\pi = \frac{d}{L}\frac{\lambda}{r_x n_x^3 - r_y n_y^3} \tag{4.17}$$

---

[4]In contrast to the linear electro-optical effect the quadratic electro-optical effect or Kerr effect is proportional to the square of the electric field.

[5]usually they are called ordinary and extraordinary beam. The one which is faster with respect to other is called "fast axis" where else the other one is called "slow axis".

denotes the half-wave plate voltage. At this voltage the phase difference between the ordinary and extra ordinary beam equals to π and therefore the Pockels Cell acts as a half-wave plate. In equation 4.16 we also use that $E = \frac{V}{d}$ and $\Phi_0 = \frac{2\pi}{\lambda}(n_x(0) - n_y(0))L$.

One can also see that the phase retardation scales linearly with the applied voltage. It is important to know that this is only valid as long as the polarization of the input wave is not parallel with the optical axis of the crystal. As an example let's assume that the fast axis of the Pockels Cells is aligned along $+45°$ and the input polarization is $+45°$. In this situation the polarization state will remain unchanged but the beam will experience a phase change proportional to the applied voltage.

Pockels Cells as Phase Modulators

This phase change only occurs for input polarization components parallel to the fast axis of the crystal. The amount of phase shift for this polarization components can be written as [44]:

$$\varphi = \frac{2\pi n(E)L}{\lambda} \tag{4.18}$$

By using equation 4.14 this evolves to

$$\varphi = \varphi_0 - \frac{\pi r n^3 E L}{\lambda} \tag{4.19}$$

were $\varphi_0 = \frac{2\pi n L}{\lambda}$ denotes the phase change in absence of an electric field. Again one can use the same trick as before and write $E = \frac{V}{d}$. Then equation 4.19 becomes

$$\varphi = \varphi_0 - \pi \frac{V}{V_\pi} \tag{4.20}$$

where

$$V_\pi = \frac{d\lambda}{L r n^3} \tag{4.21}$$

is called the half-wave plate voltage at which the phase shift equals to π. This result is similar to equation 4.17, but in this case the input polarization is parallel to the fast axis of the Pockels Cells and therefore the term $r_y n_y^3$ vanishes. Again the relation between the applied voltage and the amount of phase change is linear and only those polarization components parallel to the optical axis of the crystal experience this phase change. We used this effect to realize the interferometrical switchable beam splitter.

Specifications of the Pockels Cells

Our crystals are manufactured by the company *Leysop LTD* and are made of RTP (Rubidium Titanyl Phosphate). Every Pockels Cell consists of two crystals which are mounted
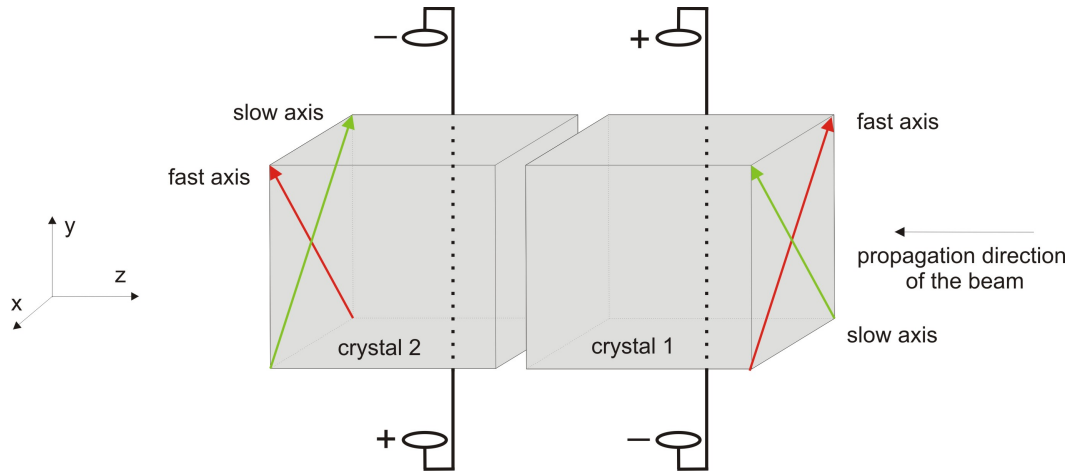
Figure 4.8.: *A schematic diagram of the Pockels Cells. The voltage on the first crystal has opposite polarity to the second one. Therefore the optical axis are complementary to each other. The advantages of this structure are described in the text.*

in series to the optical path (see figure 4.8). The light propagates in z-axis and the voltage is applied in the y-axis. The crystals are oriented in such a way, that the fast axis of the first one becomes the slow axis of the second one. This arrangement has two advantages:

- First, the static birefringence of the two crystals is automatically compensated. But when the voltage is applied, the induced birefringence adds up because the electric field has opposite polarity for each crystal.

- Secondly both crystals are electronically switched in parallel. Therefore the voltage needed for a 90° polarization switch can be halved compared to a single unit.

The product specifications are given in table 4.1.

Model	RTP-4-20
Aperture crystal dimensions	4mm
Total crystal length (2crystals)	20mm
Approximate half wave voltage (1064nm)	1.3kV
Typical dynamic extinction ratio (1064nm)	>200:1
Typical capacitance	6pF
Peak damage threshold (1064nm, 1ns pulse)	$> 1GWcm^{-2}$
Insertion loss	$< 2\%$
Physical dimensions (mm)	35x55

Table 4.1.: The RTP crystal specifications (taken from www.leysop.com).

Optical alignment of the Pockels Cells

In order to achieve a good switching contrast, one has to align the Pockels Cells well. This was done by observing isogyre patterns [45]. An interference picture as you can see in figure 4.10 occurs if a divergent beam propagates through a birefringent medium which is placed between two crossed polarizers. A schematic picture of this alignment setup can be seen in figure 4.9.
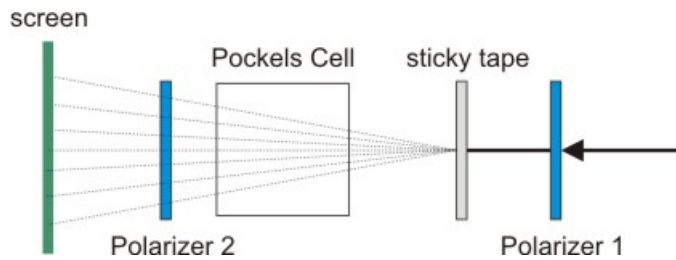

Figure 4.9.: *Setup for adjusting the crystal orientation in the Pockels Cells with isogyre patterns. Two polarizers are aligned orthogonal to each other. The sticky tape scatters the beam such that it diverges on its way through the Pockels Cells. The interference pattern is recorded by on screen. For a detailed description see text.*
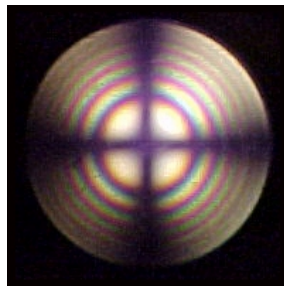

Figure 4.10.: *An isogyre pattern for an unaxial calcite crystal which is optimally aligned. In this case the input beam is parallel to the optical axis. (Figure taken from http://www.uwgb.edu/dutchs/petrolgy/intfig1.htm*

The first polarizer ensures that the input polarization is well defined (for example +45°). The transparent sticky tape scatters the beam such that it diverges. One could also use a lens, but in our case it was easier to use a sticky tape. Then the beam travels through the electro-optical modulator where the polarization state is rotated. The second polarizer is aligned orthogonal to the first one (in our case -45°). Finally the laser is visualized on a screen (for instance a piece of paper).

The reason why this interference pattern appears is the following: Every polarization input will be rotated in the birefringent medium symmetrically around the optical axis of the crystal, except those that are exactly polarized along this axis. Those photons

will remain their polarization and are absorbed by the second polarizer. A beam whose polarization is forming an angle with the fast or the slow axis of the crystal will undergo a polarization rotation. Therefore its state has some components parallel to the second analysing polarizer and will not be erased completely. The observed isogyre patterns are characteristic for the orientation of the central beam relative to the optical axis of the crystal. As one can see from figure 4.10 the isogyre patterns form a dark cross surrounded by light. The dark concentric rings are formed by interference. Due to the scattering every beam takes a different path through the crystal and therefore experiences different phase shifts which leads to this interference.

Figure 4.10 shows the image of a well aligned Pockels Cell. If the incident beam is not parallel to the optical axis one will see different isogyre patterns as seen in figure 4.11. Accordingly one has to rotate and tilt the crystal inside the driver box until the isogyres are optimized. In first approximation this can be done by hand. Afterwards one has to use the adjustment screws inside the Pockels Cell to fine tune the alignment (see figure 4.12).
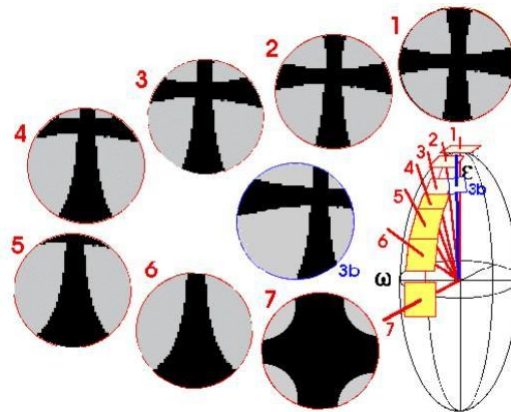

Figure 4.11.: *Different isogyre patterns for different orientations of the crystal axis with the incoming beam polarization. The first situation corresponds to the situation where the beam is parallel to the optical axis of the crystal. In this case the indicatrix (right hand side of the picture) forms a circle and the isogyre pattern shows the good alignment. In all the other cases the input beam is not parallel to the optical axis and therefore the indicatrix forms an ellipse. Picture taken from http://edafologia.ugr.es*

Since our laser emits light at 808 nm we had to use an infrared viewer in order to observe the isogyre patterns. The resolution of these devices is rather low so we aligned the crystal as good as we could with this method and then changed to a different procedure.

To test the alignment of the Pockels Cell we removed the sticky tape and monitored the transmitted laser intensity with a photo diode. The polarizers remained orthogonal but where rotated to H and V basis. If the Pockels Cell is not operating the photo diode will register no intensity because the light is absorbed by the second polarizer. But if the
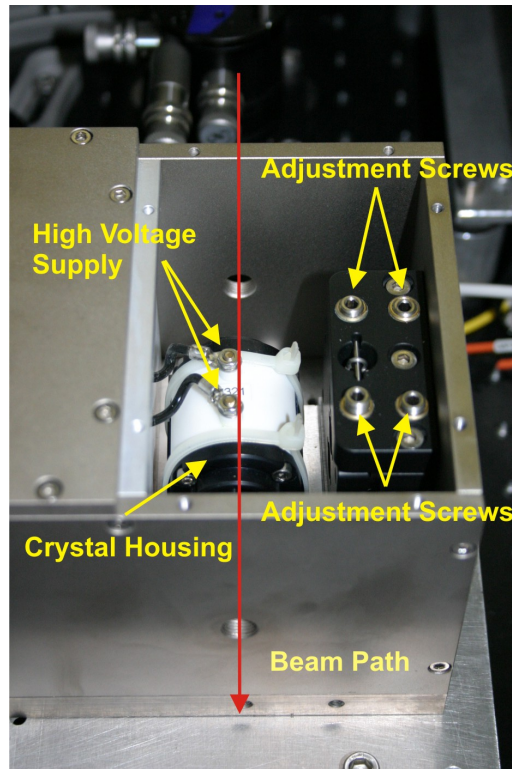
Figure 4.12.: *A Pockels Cell mounted inside a driver box. The crystal can be translated and tilted with four adjustment screws.*

crystal is aligned in 45° and a half-wave voltage is applied the polarization input state will be rotated to the orthogonal basis and therefore be completely transmitted through the last polarizer.

At first we set both polarizers to parallel and monitored the maximum intensity on an oscilloscope. Then we rotated the second polarizer by 90° and optimized the transmittance by slowly increasing the voltage. The half-wave voltage was found at $1,06 \pm 0.02 kV$. Afterwards we fine tuned the crystal orientation with the four adjustment screws inside the Pockels Cell (see figure 4.12).

Operation of the Pockels Cell driver

To operate a Pockels Cell it is necessary to supply it with a proper high voltage On - Off signal. Our electronics system was manufactured by the company *Bergmann Meßgeräte KG* and consists of a high voltage supply, a splitter box and a driver box.

A so called "splitter box" (see figure 4.14) uses a reference TTL signal as input (in our case 2.5 MHz produced by a function generator) and generates four output pulses (*A-On, B-On, A-Off, B-Off*) which are operating in a double push pull switch scheme. A circuit

diagram of this can be seen in figure 4.13. A *A-On* signal closes the high voltage cycle to the crystal while a detected *B-On* pulse opens it again. Likewise *B-Off* injects the high voltage to the crystal and *A-Off* stops it. In order not to damage the switching system, the minimum time difference between a *A-On* and *A-Off* signal and *B-On* and *B-Off* respectively, has to be larger than 50 ns.
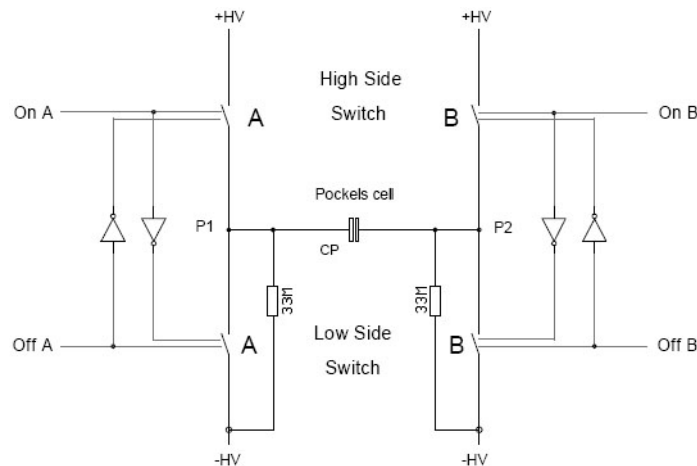
Figure 4.13.: *Schematic diagram of a push pull switch. A signal from A-On closes the High Side Switch A circle and opens the Low Side Switch A circle. A A-Off signal opens the High Side Switch A and closes the Low Side Switch. The B side operates in the same regime. (Figure taken from Fast Splitter Manual BME FSP01, Bergmann Meßgeräte KG, http://www.bme-bergmann.de)*

Figure 4.14.: *A picture of a so called "splitter box" from the company Bergmann Meßgeräte KG. The input signal can be gated with another signal e.g. from a quantum random number generator (QRNG). The four output connectors on the left hand side transmit the control signals to the Pockels Cell. The On time of the Pockels Cell can be adjusted by several switches inside the "splitter box".*

Figure 4.15.: *Observation of the Pockels Cells response time, which switches the phase inside the MZI. Shown is the intensity of a strong laser pulse which is switched from minimum to maximum (from one output to the other) due to the phase shift from the Pockels Cells. The green and blue lines denote the 10% and 90% level of the rising and falling edges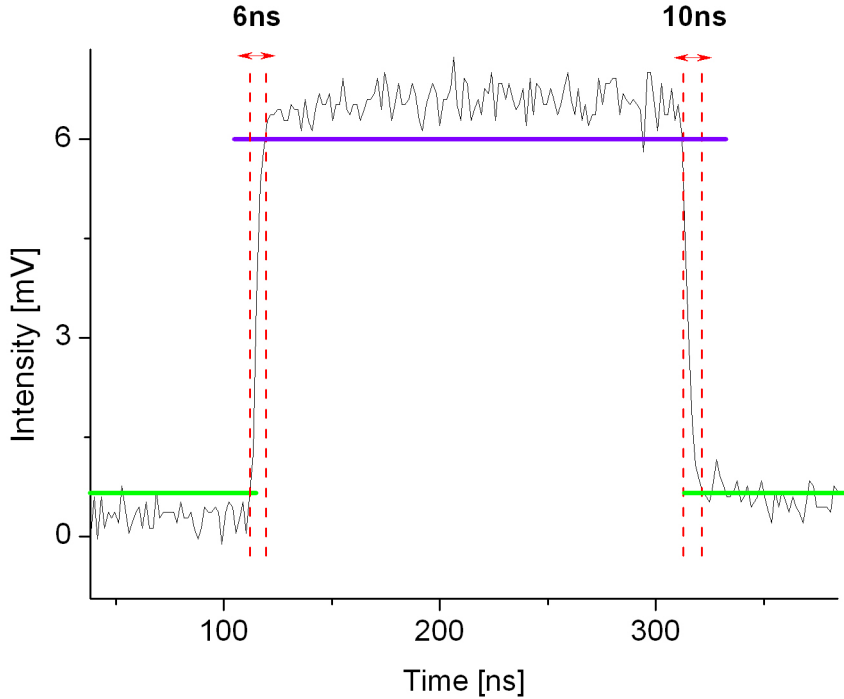. From this picture we can see that the rising time of our Pockels Cell is 6 ns whereas the falling time is approximatly 10 ns.*

These four TTL signals plus the high voltage supply are plugged into the driver box. The effective On time of the Pockels Cell (time difference between *A-On* and *B-On* or *A-Off* and *B-Off*) can be freely set inside the splitter box (see figure 4.14). The rise time of our Pockels Cells was measured by observing the phase switching on an oscilloscope. We used the 10% and 90% levels of the rising and falling edges of the signal to calculate the rise and fall time from the collected data (see figure 4.15). The different operation modes of the push pull switch can be seen in figure 4.16. One Pockels Cell in our interferometer is operating in unipolar positive mode and the other one in unipolar negative mode. If the two Pockels Cells were using the same switching mode both arms of the Mach-Zehnder would experience the same phase shift and therefore get canceled. If you want both phase shifts to be summed up their sign has to be opposite.

Unipolar Positive Mode
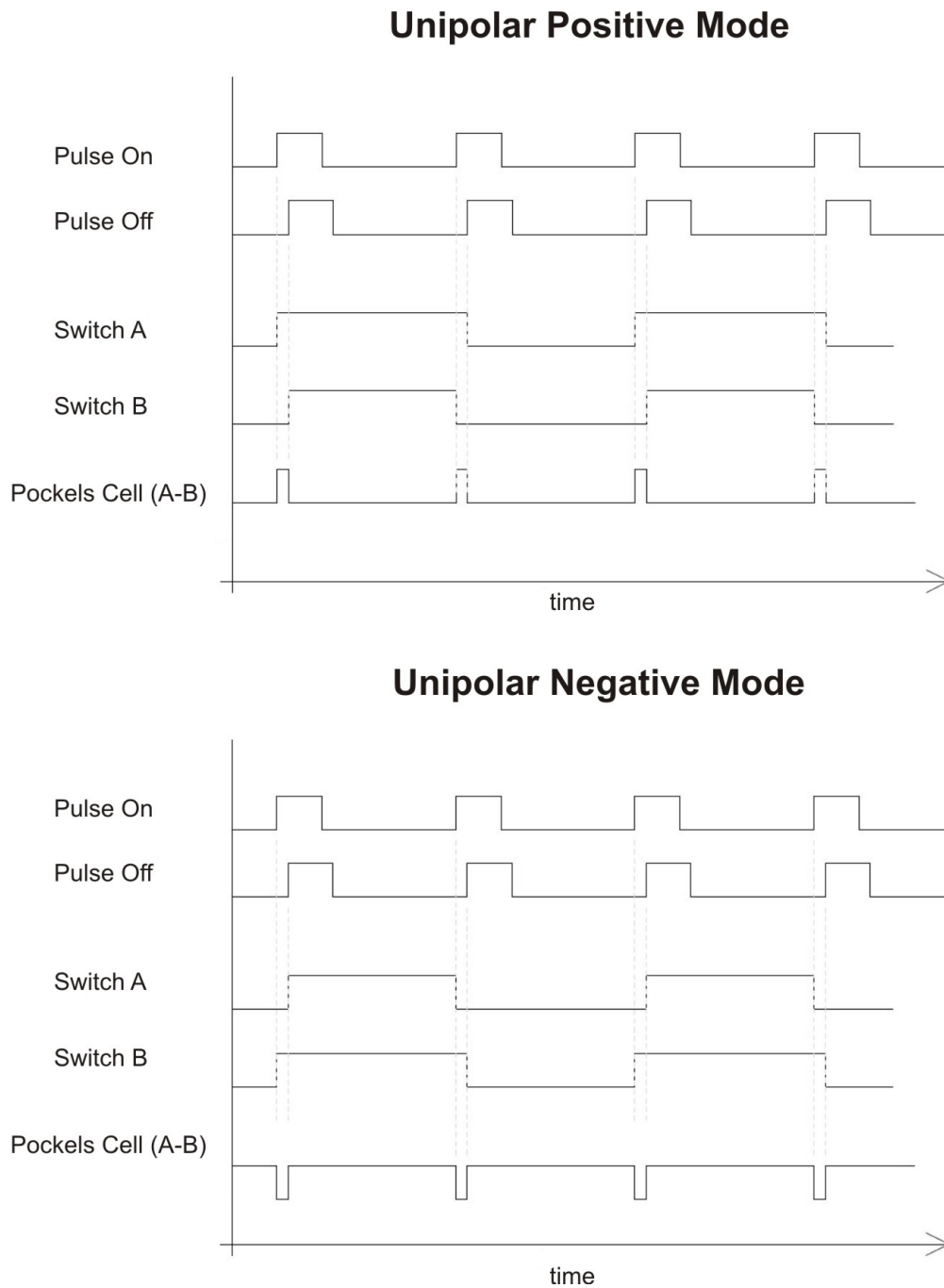

Unipolar Negative Mode

Figure 4.16.: *Different operation modes of the Pockels Cells. There are two additional operation modes (Alternating Mode A and Alternating Mode B) which are not shown here, because we do not use them in our experiments. (Figure taken from Fast Splitter Manual BME FSP01, Bergmann Meßgeräte KG, http://www.bme-bergmann.de)*

4.2.5. Experimental Test with Heralded Single Photons

So far we have seen that the interference visibility and the alignment of the Pockels Cells is very good. Now we had to test the performance of our polarization independent fast tunable beam splitter (TBS) with single photons, since this is what we are interested in. We did that by using time-entangled photon pairs (see chapter 3.2). We heralded the presents of a photon in the Mach-Zehnder by the detection of its twin. Then we used the detection signal to trigger the Pockels Cells and switched the phase of the heralded single photon. This experiment was performed to show that our setup really works as a polarization independent fast tunable beam splitter and to check how good the switching contrast can be (tuning range of the splitting ratio).

The setup for this experiment can be seen in figure 4.17. The collinear photon pair source (see chapter 3.2) emits an orthogonal polarized photon pair (H/V) at 808 nm. The photons are emitted into the same spatial mode and separated from each other on a PBS. One photon passes a 3 nm interference filter before it is coupled into a single-mode fiber and guided to a detector. The other one is coupled into a 100 m single-mode delay fiber before it enters the interferometer.

We had to delay this photon because the signal from the detection event of its twin has to be guided to the splitter box where it triggers the EOMs. The signal processing takes approximately 150 ns. During this time the heralded photon has to be stored in the delay fiber. Otherwise it would pass the Mach-Zehnder before the Pockels Cell can be switched. The time delay of the 100 m single-mode fiber is about 500 ns which is actually much more than required. A shorter delay fiber would have been enough for this experiment, but we bought this fiber for the delayed-choice entanglement swapping experiment where we are going to need a longer delay. The time delay adjustment is very crucial and was achieved with our home-built FPGA Logic.

The UV pump power was attenuated to 250 mW to avoid higher-order emission from the spontaneous parametric down conversion source. We detected approximately 240.000 singles in each arm and 20.000 coincidences between them.

One important feature of our TBS is polarization independence. In order to show that, we had to be able to rotate the polarization of the photon before entering the Mach-Zehnder. We achieved that with one Bat-ear polarization controller on the single mode input fiber.

Before we turned on the EOMs we locked the phase of the interferometer with our PID regulator such that the count rate of one output detector was maximized and the other one was minimized. Afterwards we increased the voltage on both Pockels Cells slowly and measured the coincidence events between detector 1 and 2 with the trigger photon. Depending on the applied voltage, the splitting ratio can be changed. The results of such a measurement can be seen in figure 4.18.
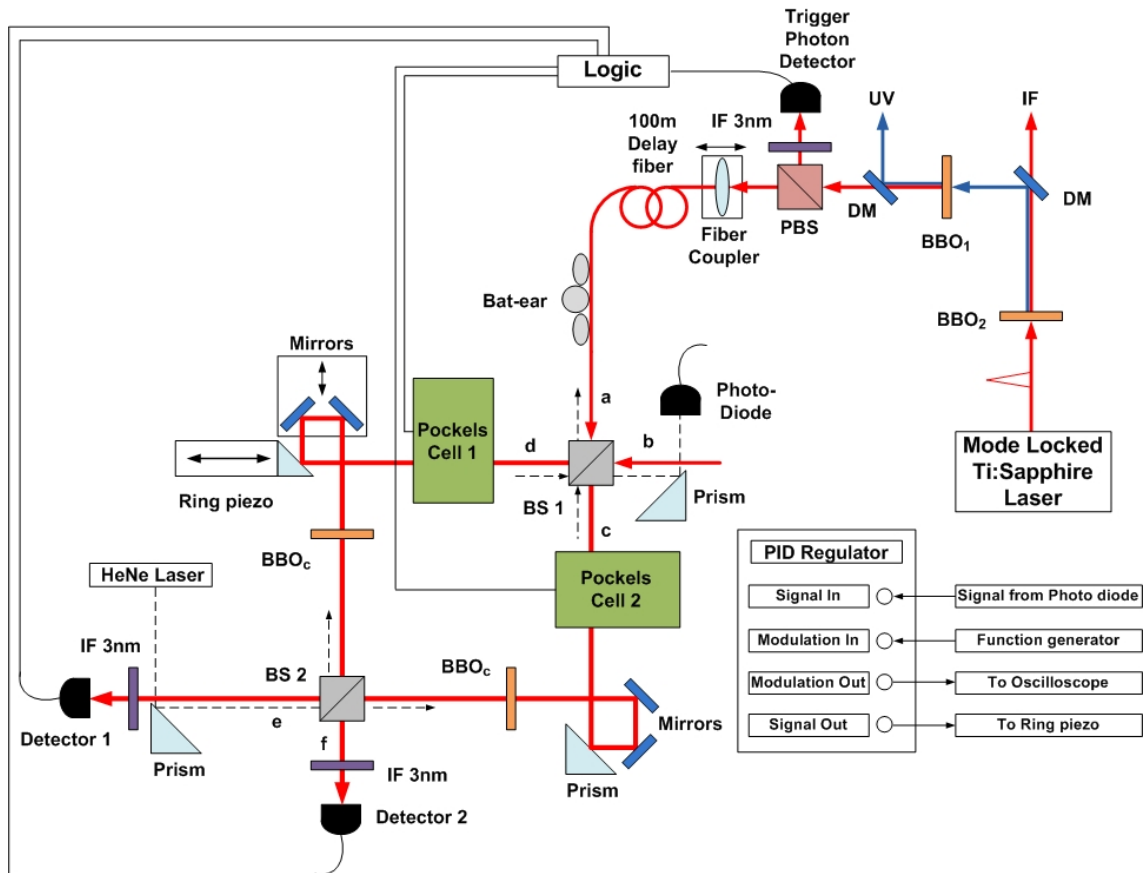
Figure 4.17.: *A schematic diagram of the setup which is used to test the performance of our tunable beam splitter (TBS). A mode locked Ti:Sapphire Laser emits femtosecond pulses at 808 nm. These pulses are up-converted to 404 nm via a SHG crystal (BBO2). The remaining infrared beam is separated from the UV by a dichroic mirror (DM). The UV pulse is focused into a Type-II down-conversion crystal (BBO1) which is aligned for collinear phase-matching. The correlated photons are separated on a polarizing beam splitter (PBS). One of the photons is used to herald the presence of its twin and to trigger the Pockels Cells. The other one is coupled into a 100 m single-mode fiber before it is guided to one of the input modes of the Mach-Zehnder (a or b). The Bat-ear polarization controller is used to rotate and adjust the polarization of the photons inside the fiber. The tunable beam splitter is realized by a Mach-Zehnder interferometer (two beam splitters (BS1 and BS2) and several mirrors and prisms) with one Pockels Cell in each arm. The incoming photon gets a voltage dependend phase-shift from the Pockels Cells. In this way we can tune the splitting ratio of the effective beam splitter. The active phase-stabilization and phase-locking is achieved by a HeNe laser which counter propagates through the setup and creates a reference signal on a photo diode. This signal is send to a PID regulator which controls a ring piezo inside the interferometer. Two BBO crystals (BBOc) inside the Mach-Zehnder compensate some unknown birefringence which limits the visbility in +/- basis. 3 nm interference filters (IF) and single-mode fibers at the output couplers gurantee good spectral and spatial filtering.*
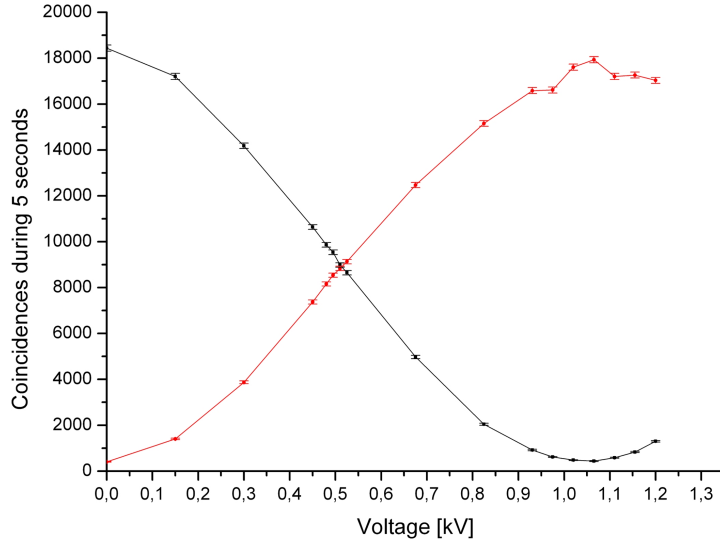
Figure 4.18.: *A typical measurement results for polarized photons on input coupler a or b. The black (red) dots denotes the coincidences between detector 1 (detector 2) and the triggering detector outside photon from the down-conversion. The measurement points are connected by a line to show the next point. The x-axis represents the Pockels Cell voltage and corresponds to the amount of phase-shift. The error bars are calculated from the counting statistics. This measurement shows an H polarized photon in input mode a.*
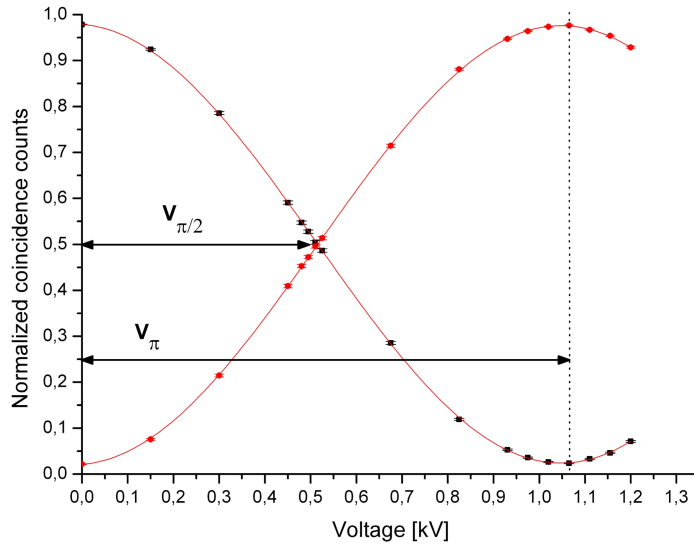
Figure 4.19.: *Here the coincidences from figure 4.18 are normalized by the sum of the co-incidence counts from both detectors and fitted with a sin function. From the fitting results we can read out the switching visibility: contrast from minimum to maximum to be $95,2 \pm 0,1\%$ for det1 (black dots) and $95,9 \pm 0,2\%$ for det2 (red dots). We can also read out the $\frac{\pi}{2}$ and π voltage. The results for other polarizations and for input mode b are given in table 4.2.*

We also normalized the counts to the sum of the detected coincidences and fitted the resulting curves with a sinusoidal function (see figure 4.19).

The calculated visibilities for every polarization from input mode *a* and *b* are given in table 4.2. From the measurement results one can also read out the voltage dependence i.e. where the π and $\frac{\pi}{2}$ shift can be found. These results are also given in table 4.2.

Polarization input a	Visibility detector 1 [%]	Visibility detector 2 [%]	π phase shift voltage [kV]	$\frac{\pi}{2}$ phase shift voltage [kV]
Horizontal	$95,2 \pm 0,1$	$95,9 \pm 0,2$	$1,06 \pm 0,04$	$0,51 \pm 0,04$
Vertical	$95,9 \pm 0,4$	$100 \pm 0,4$	$1,06 \pm 0,04$	$0,46 \pm 0,04$
+45°	$95,4 \pm 0,3$	$97,9 \pm 0,4$	$1,06 \pm 0,04$	$0,51 \pm 0,04$
-45°	$95,4 \pm 0,3$	$96,6 \pm 0,4$	$1,15 \pm 0,04$	$0,58 \pm 0,04$

Polarization input b	Visibility detector 1 [%]	Visibility detector 2 [%]	π phase shift voltage [kV]	$\frac{\pi}{2}$ phase shift voltage [kV]
Horizontal	$94,5 \pm 0,3$	$96,4 \pm 0,6$	$1,06 \pm 0,04$	$0,55 \pm 0,04$
Vertical	$97,8 \pm 0,8$	$95,8 \pm 0,3$	$1,06 \pm 0,04$	$0,49 \pm 0,04$
+45°	$96,3 \pm 0,3$	$96,3 \pm 0,5$	$1,06 \pm 0,04$	$0,55 \pm 0,04$
-45°	98 ± 1	$96,4 \pm 0,3$	$1,06 \pm 0,04$	$0,51 \pm 0,04$

Table 4.2.: Measurement results for input mode a upper table and input mode b lower table. π phase shift denotes the voltage where the photons are switched from minimum to maximum and vice versa. Otherwise the $\frac{\pi}{2}$ phase shift tells us where the setup operates as a switchable beam splitter. Ideally V_π should be 2 times $V_{\frac{\pi}{2}}$, because the Pockels Effect is a linear optical effect. From the results one can see that this criteria is fullfilled within the measurement errors.

At this point it is very important to understand what happens with the input state inside the Pockels Cells. As we know from chapter 4.2.4 a +45° or -45° polarized beam will only experience a phase shift proportional to the voltage, if the crystals are aligned in 45° basis. We also know that the amount of phase shift on both EOMs is summed up in the interferometer. Therefore we would expect a total π shift if both crystals operate at $\frac{\pi}{2}$ voltage. But one can see from our measurement results that a full π phase shift is only accomplished if a half-wave plate voltage is applied to each Pockels Cell[6]. Why is that?

As explained, our EOMs contain two crystals (see figure 4.8) which are aligned in such a way, that the fast axis of the first crystal becomes the slow axis of the second one. If the input polarization is in parallel to the fast axis of the first crystal it will only experience a phase shift on this crystal and not on the second one. Therefore the phase is only shifted by $\frac{\pi}{2}$ if a half-wave plate voltage is applied.

If the photon is polarized in H or V it will experience a phase shift at both crystals,

---

[6]We found the half-wave plate voltage at $1.06 \pm 0.02 kV$ (see chapter 4.2.4).

because H and V can be written as a superposition of $|+\rangle$ and $|-\rangle$.

$$|H\rangle = \frac{1}{\sqrt{2}}(|+\rangle + |-\rangle) \tag{4.22}$$

$$|V\rangle = \frac{1}{\sqrt{2}}(|+\rangle - |-\rangle) \tag{4.23}$$

Consider that a half-wave plate voltage is applied to the Pockels Cells and the beam polarization is horizontal. Then the photon will undergo a $\frac{\pi}{4}$ phase shift on each crystal which is summed up to $\frac{\pi}{2}$ in total. Besides that the polarization is switched from H to V but since the polarization in both arms of the Mach-Zehnder is switched, this effect does not harm our interference visibility.

Conclusion

The measurement data shows that we experimentally realized a polarization independent fast optical beam splitter by placing one EOM in each arm of a Mach-Zehnder interferometer. The splitting ration can be controlled by the voltage which is applied to the Pockels Cells. The maximal switching visibility is above 95% for every input polarization and also the voltage dependence is roughly the same. This proofs the excellent perfomance of our setup.

This device can also be used for quantum teleportation [22], entanglement swapping [25], one-way quantum computation with active feed forward [46] and many others.

5. Two-Photon Interference on the Switchable Beam Splitter

Another step towards the realization of delayed-choice entanglement swapping experiment was to performe a Hong Ou Mandel dip measurement with our fast interferometric switchable beam splitter. It was necessary to show that our TBS is able to realize a switchable Bell-state analyzer.

But this test experiment is also interesting from a more fundamental point of view. By triggering the Pockels Cells with a quantum random number generator (QRNG see appendix B) which was located in another Lab (40 m away from the setup) we were able to perform a "delayed-choice HOM measurement". The fact that the TBS and the QRNG were space-like separated in the experiment, guaranteed that Einstein's locality condition was fulfilled. In that way we can extend Wheelers "delayed-choice gedankenexperiment". We show that complementarity between interference and which-path information is valid not only for one-photon interference but also in the two-photon case. This complementarity is also independent from the space time arrangement between the photon entry of the interferometer and the choice whether to use the beam splitter or not.

5.1. Hong Ou Mandel interference

In 1987 Hong Ou and Mandel (HOM) introduced a way to measure the time difference between two photons on a sub picosecond scale [47] by a fourth-order quantum interference effect. Today their observation plays an important role in quantum information processing because of its possibility to realize a Bell-state measurement (see appendix C).

Consider a 50:50 beam splitter with two input modes a, b and two outputs c, d. There are four possibilities for the two photons to behave (see figure 5.1). If the photons are indistinguishable in every parameter their detection event in the output modes does not allow to determine the origin of the photon (mode a or b). Therefore case 2 and 3 vanish and one will not observe any coincidence events between the two output detectors.

Mathematically one can describe this phenomenon in the following way: The initial state can be described as

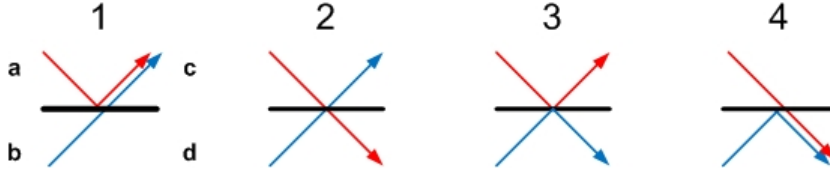$$|\Psi_0\rangle = \widehat{a}_a^t \widehat{a}_b^t |0\rangle \tag{5.1}$$

Figure 5.1.: *If two photons enter a symmetric 50:50 beam splitter there are four possible
outcome scenarios. One photon gets reflected and the other one is transmitted
(case 1 and 4). Both photons get reflected (case 3) or transmitted (case 2).*

where $|0\rangle$ denotes the vacuum state and $\widehat{a}_a^t \widehat{a}_b^t$ are the creation operators acting on mode
$|a\rangle$ and $|b\rangle$. In this calculation I will assume that the photons are indistinguishable. By
using equation 4.2 the state after the beam splitter evolves to

$$|\Psi_1\rangle = \frac{1}{2}(\widehat{a}_c^t - i\widehat{a}_d^t)(\widehat{a}_d^t - i\widehat{a}_c^t)|0\rangle \tag{5.2}$$

By using the definition of the commutator $[a, b] = ab - ba$ one can rewrite this as

$$|\Psi_1\rangle = \frac{1}{2}(-i\widehat{a}_c^{t2} - i\widehat{a}_d^{t2} + [\widehat{a}_c^t, \widehat{a}_d^t])|0\rangle \tag{5.3}$$

Since the commutator between different photon modes vanishes, the final state becomes

$$|\Psi_1\rangle = -\frac{1}{2}(i\widehat{a}_c^{t2} + i\widehat{a}_d^{t2})|0\rangle \tag{5.4}$$

One can see that both photons will always exit into the same output (case 1 and 4) and
therefore one will not observe any coincidence detection events between the detectors in
mode c and d.

Quantum physics predicts a maximum interference visibility for a Hong Ou Mandel Dip
of 100% [47] whereas the classical limit is 50% [48].

There are many experimental effects that limit the interference visibility i.e. polarization
alignment, center wavelength mismatch, spatial overlapping on the beam splitter, coherence
length, amplitude difference and time difference between the two entering events. A precise
calculation about how these effects limit the interference visibility can be found in [49].

5.1.1. Alignment of the setup

Hong Ou Mandel interference was originally introduced as a method of measuring time
differences between two photons on a subpicosecond scale. In order to observe a dip in
the coincidence counts one has to vary the arrival time between the two photons on a
beam splitter around the 0 time difference position. Finding the point where both photons
arrive at the same time is not easy since the whole travel path of both photons, until they

meet on a beam splitter, has to be the same within μm. The Dip width depends on the coherence length of the photons and is defined by the spectral filtering.

Here I want to present two different methods which are useful for finding a HOM dip position. A schematic picture of the alignment setup can be seen in figure 5.2. The down-conversion source was the same as in chapter 4.2.5, but this time we guided both photons, over 100 m single-mode fibers, to the input couplers of the Mach-Zehnder. We installed these delay fibers because we needed them for the next experiments and of course the final delayed-choice entanglement swapping experiment.
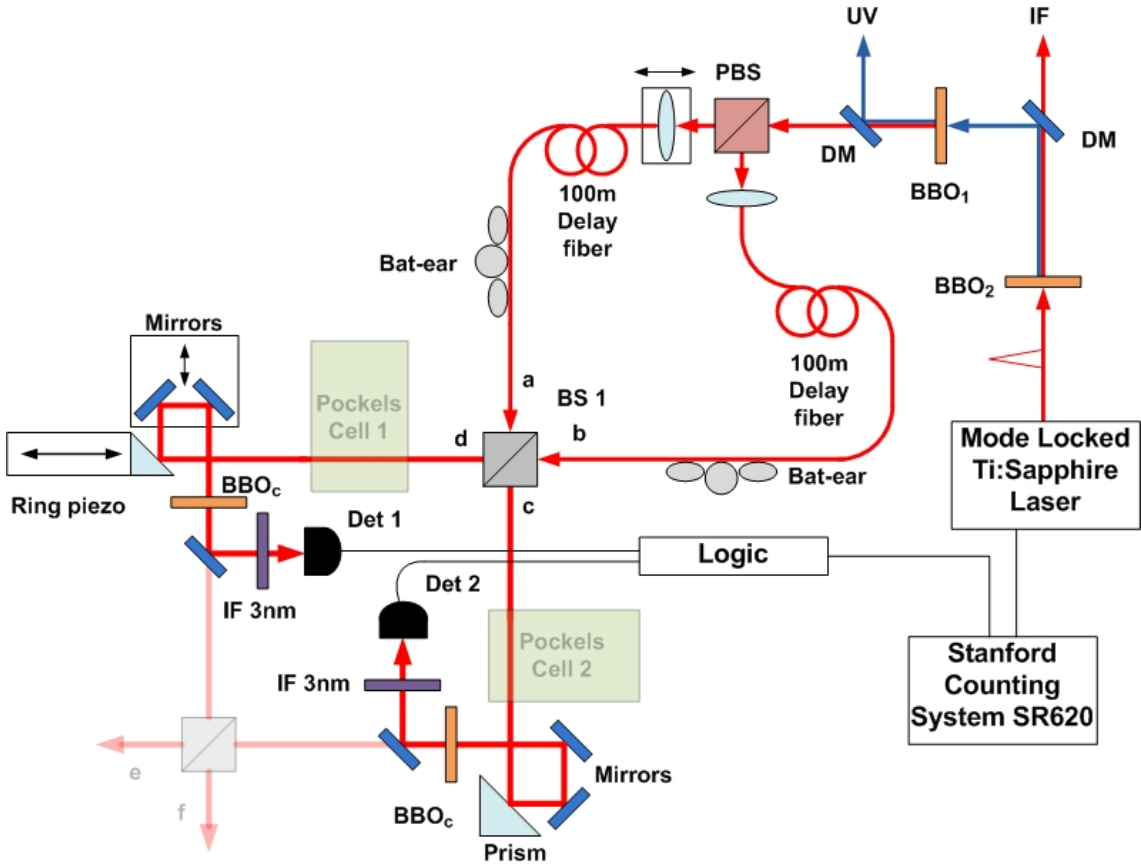
Figure 5.2.: *The setup for the alignment of the delay between the two photon's entry of the MZI. The collinear photon pair source is still the same as in chapter 3.2. A timing analyzer (SR620) is used to measure the relative times of the photon detection with respect to the Laser pulse emission. Both down conversion photons are coupled into 100 m delay fibers before entering the switchable beam splitter setup. One coupler is mounted on a translation stage to vary the travel time of this photon. The polarization adjustment was done with two bat ears. Inside the Mach-Zehnder we placed some additional mirrors and fiber couplers to get the photons out before they reach the second beam splitter.*

In our case the HOM dip position is defined by the path length difference between the two photons from the PBS after the source over the 100 m single-mode fibers until the first beam splitter BS1 in the Mach-Zehnder (see figure 5.2). One of the couplers, which couples the down-conversion photon into the delay fiber, is mounted on a translation stage (see figure 5.2). The refractive index of a glass fiber is around 1.5 and therefore the light velocity inside a fiber is approximately 1/3 slower than in air. This velocity difference between fiber and air can be used to vary the arrival time at BS1 of one photon with respect to the other. The second beam splitter BS2 is not important because the two arms of the interferometer have no path length difference. For the alignment we were interested in finding the 0 time difference for both photons from the PBS to BS1. Therefore we coupled the two photons out of the setup and detected them with an APD immediately after BS1 (additional mirrors and couplers can be seen in figure 5.2). By using this trick, we did not care about the phase locking or the Pockels Cells.

As a first approximation we measured the arrival time difference with a *Stanford Counting System SR620*. This device measures time differences between TTL pulses in tenth of picoseconds range. We blocked one fiber coupler from the source and registered the time difference between the TTL pulse from the laser[1] and the TTL signal from the detector. Then we blocked the other coupler at the source and measured the difference for the other input arm. Afterwards we moved the motorized fiber coupler forwards or backwards until the time difference between laser pulse and detection signal was the same for both inputs.

This method is only a first approximation because it is very sensitive to any electronic delays and shifts. Even more critical is the trigger level inside the counter. But to our knowledge it gives an accuracy within a 5 cm range around the dip.

From here, one can only move the coupler with the motorized stage and register the coincidences counts after the beam splitter as a function of the position and perform a HOM dip measurement. If this HOM dip scan passes through the 0 time delay region, one will observe the typical HOM dip interference pattern in the coincidence count rate (see figure 5.3).

To guarantee that the center frequencies are the same for both down-conversion photons we used 3 nm bandwidth filters before the couplers (see figure 5.2). Although the count rate dropped by approximatly 50%, those filters enhanced the coherence length of the photons and therefore the visibility of the dip improved. The polarization of the two photons had to be same and was adjusted with one bat ear on each input fiber.

This HOM dip alignment experiment was performed to find the exact delay of the photons entering the BS1 in the MZI.

---

[1]Our Chameleon Laser System has a BNC output connector to read out the laser pulse signal.

Static HOM Interference on the Switchable Beam Splitter

The next step was to perform a HOM interference measurement one the whole TBS. Therefore we removed the additional fiber couplers and mirrors before BS2 and scanned another HOM dip while the phase of the Mach-Zehnder interferometer was locked such that the whole setup worked as one big statical beam splitter. In this measurement the Pockels Cells were Off and it was performed to adjust the setup and to see what kind of visibility and count rate we can expect. The result can be seen in figure 5.3.

We attenuated our Laser such that the UV power was about 300 mW. In this way we could avoid most of the higher-order emission from the crystal and gained a better visibility. The coincidence count rate dropped from around 20.000 produced by the source to 500 outside of the dip. The reason for this is that we used 3 nm interference filters after BS2 and single-mode fibers to couple the photons out of the MZI. All of this increased the visibility but decreased the count rate dramatically.
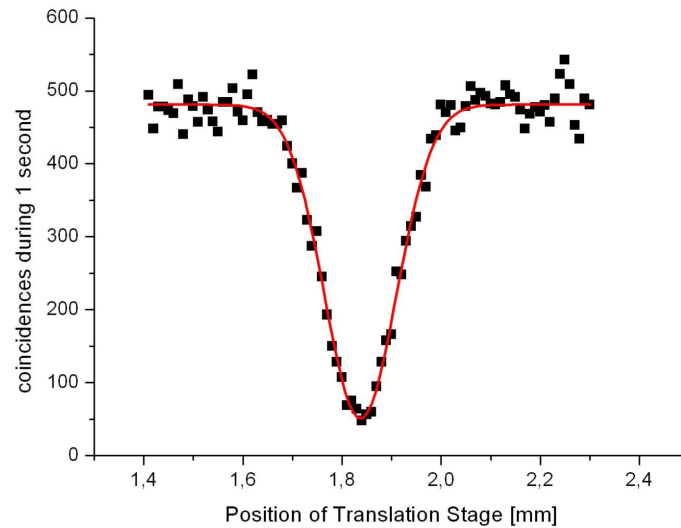
Equation	$y = A*(1+B*\exp(-((x-C)/D)^2/2))$		
Adj. R-Square	0,9794		
		Value	Standard Error
	A	481,24718	2,80053
	B	-0,89409	0,01428
	C	1,83716	0,00134
	D	0,07269	0,0015

Figure 5.3.: *A result of a test measurement to find the HOM dip position and to align the setup. The coincidence count rate (black dots) is fitted with a HOM dip function, which can be seen in the table below. The data shows that the visibility of this dip is $89 \pm 1\%$.*

5.1.2. HOM Interference on the Switchable Beam Splitter

In this experiment we use our fast interferometric switchable beam splitter to show complementarity in a two-photon experiment under Einstein's locality conditions. We can show that the complementarity between interference and which-way information is valid not only in the one-photon but also in the two-photon case and that this complementarity is independent from the space time arrangement of the choice with respect to the photon entry in the MZI. Therefore we triggered the Pockels Cells with a QRNG placed in another Lab 40 m away from the source and the TBS (see figure 5.4). We did the same measurement in 3 different space time scenarios namely, choice and setup space-like separated, choice in the past-light cone of the source and choice in the future-light cone of the source. We could not observe any fundamental differences between the 3 measurement results.
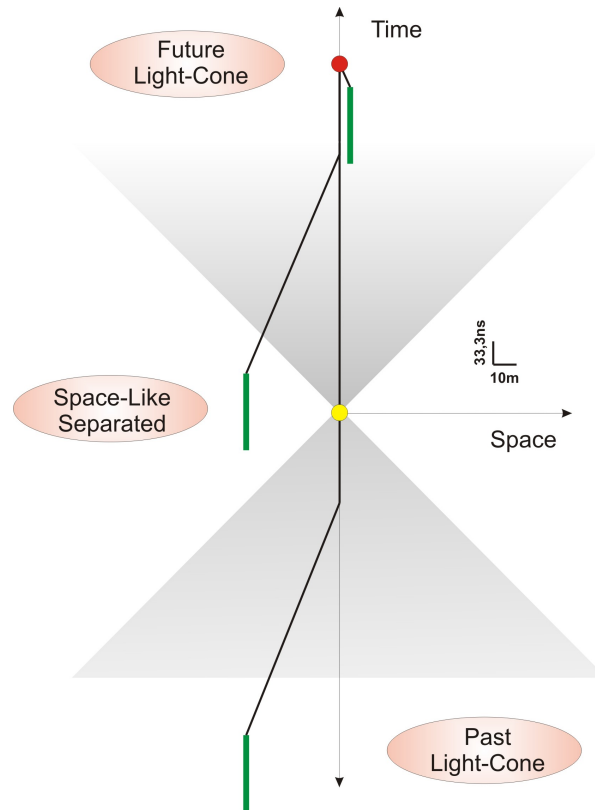
Figure 5.4.: *A space-time diagram for all three measurement scenarios in the delayed choice HOM interference experiment. The yellow dot symbolizes the production event of the photon pair, while the red point represents the entry into the interferometer. The choice (green bar) is drawn as a series of events (for explanation see appendix B). In the space like separated and in the past light-cone case our choice-maker was located in another room 40 m away from the source. Whereas in the future light-cone scenario the QRNG was placed in the same Lab.*

The settings are the same as in the previous measurement, but this time we locked the phase of the Mach-Zehnder to zero, defined by maximizing the counts of detector 1 and minimizing them of detector 2. This was done by blocking one down-conversion coupler and adjusting the phase-locking point with the PID to the desired position. Then we turned on the EOMs and applied a quarter-wave plate voltage ($\frac{\pi}{2}$ phase shift) to the crystals. With this setup we are able to observe two different measurements at the same time. If the Pockels Cells are On and the whole MZI operates as a beam splitter, HOM interference between the two output modes of the TBS can be resolved. But if the EOMs are Off, the photons from input mode a (b) will always exit in mode f (e) and therefore no HOM interference can be resolved.

To proof this I want to go through the calculation which show the bunching between the two output modes e and f if a quarter-wave plate voltage is applied to the Pockels Cells. Without loss of generality we assume that the photon entering in spatial mode a is H polarized while the other one in mode b is V. The polarization of the input photons has to be opposite i.e. H and V or + and -. The reason for that can be found in the calculations bellow. Our initial state is:

$$|\Psi\rangle = |H\rangle|a\rangle \otimes |V\rangle|b\rangle = \frac{1}{2}((|+\rangle + |-\rangle)|a\rangle \otimes (|+\rangle - |-\rangle)|b\rangle) \tag{5.5}$$

After the first beam splitter the state becomes to

$$|\Psi\rangle = \frac{i}{4}((|++\rangle - |--\rangle)|cc\rangle + (|++\rangle - |--\rangle)|dd\rangle) \tag{5.6}$$

Pockels Cell 2 gives a $\varphi(V)$ phase shift on a + polarized photon in mode c while Pockels Cell 1 induces a $\varphi(V)$ phase shift on - polarized photons in spatial mode d[2].

$$|\Psi\rangle = \frac{i}{4}((\exp^{i2\varphi(V)}|++\rangle - |--\rangle)|cc\rangle + (|++\rangle - \exp^{i2\varphi(V)}|--\rangle)|dd\rangle) \tag{5.7}$$

The second beam splitter recombines the two arms and the state evolves as follows

$$\begin{aligned}|\Psi\rangle = \frac{i}{8}(&(-\exp^{i2\varphi(V)}|++\rangle + |--\rangle + |++\rangle - \exp^{i2\varphi(V)}|--\rangle)|ee\rangle \\ &+ (\exp^{i2\varphi(V)}|++\rangle - |--\rangle - |++\rangle + \exp^{i2\varphi(V)}|--\rangle)|ff\rangle \\ &+ (2i\exp^{i2\varphi(V)}|++\rangle - 2i|--\rangle + 2i|++\rangle - 2i\exp^{i2\varphi(V)}|--\rangle)|ef\rangle)\end{aligned} \tag{5.8}$$

It is easy to see that the photons will bunch when $\varphi(V) = \frac{\pi}{2}$, because only terms in spatial mode $|ee\rangle$ or $|ff\rangle$ will survive. If $\varphi(V) = 0$ the photons will anti-bunch because both input photons will always exit into different spatial modes (only terms in spatial mode $|ef\rangle$ are left in equation 5.8). If the Pockels Cells are operating at a quarter-wave voltage

---

[2]For a detailed description about the action of the Pockels Cells see previous chapters.

one will observe a typical HOM dip, but if they are OFF, one will find a flat line in the coincidence count rate between the two outputs.

A schematic diagram of the experimental setup can be seen in figure 5.5. The trigger signal for the splitter box came from a QRNG placed 40 m away from the source in another Lab. In order not to damage the Pockels Cells we gated the 30 MHz random signal with a 2,5 MHz signal from a function generator. The time needed for the photon pair to enter the interferometer was around 500 ns. The 30 MHz random signal was send via a 81 m BNC cable (corresponding to 405 ns) from one lab to the other. There was an additional 45 ns delay in the Pockels Cells drivers. The missing 50 ns time delay was adjusted carefully with our home built FPGA Logic.

In the actual experiment we used the *A-On* and *A-Off* signal from the splitter box to identify when the EOMs were ON and OFF. In this way we were able to observe both measurements at the same time and we did not need to synchronise the QRNG with the source. Therefore and because the choice-maker was space-like separated from the setup, we can exclude any hidden communication between the decision which experiment to perform and the creation process of the photon pair.

The result of such a measurement can be seen in figure 5.6. When the Pockels Cells are ON (black dots), HOM interference with $90 \pm 5\%$ shows up. If they are OFF, a constant count rate is observed, which shows no dependence to the path length (red dots). The coincidence count rate of this line is twice as much as the plateau of the HOM dip. The reason for this is simple. When the Pockels Cells are OFF, all the photons coming from one input coupler will exit in one spatial mode. Those from the other input will always end up in the opposite exit. Theoretical there is no reason why any coincidences should be lost. But when the Pockels Cells are ON and the Mach-Zehnder operates as a beam splitter, photons from both inputs have equal probability $p = \frac{1}{2}$ to exit in a specific mode. Therefore we have the same situation as in figure 5.1. There are two out of four cases that will not lead to any coincidence detection event after the beam splitter. Accordingly half of the coincidences will be lost on the beam splitter.

By adding another 100 m BNC cable (corresponding to 500 ns time delay) we pushed the decision whether to switch the Pockels Cells On or not back into the past light-cone of the source (see figure 5.4). The HOM dip visibility in this case was $89 \pm 4\%$. The visibility in the last scenario (choice in the future light-cone of the source) was $76 \pm 4\%$. This value is a bit worse than in the other 2 measurements, mainly because we had no temperature stabilization controller for our 100 m delay fibers. If the temperature inside the fiber is not stable, it will slightly change its length. Because of these drifts the HOM dip position was always moving and due to our long integration time (100 s), this led to a lower dip visibility. But still this value clearly indicates that the photons were interfering on our switchable beam splitter.
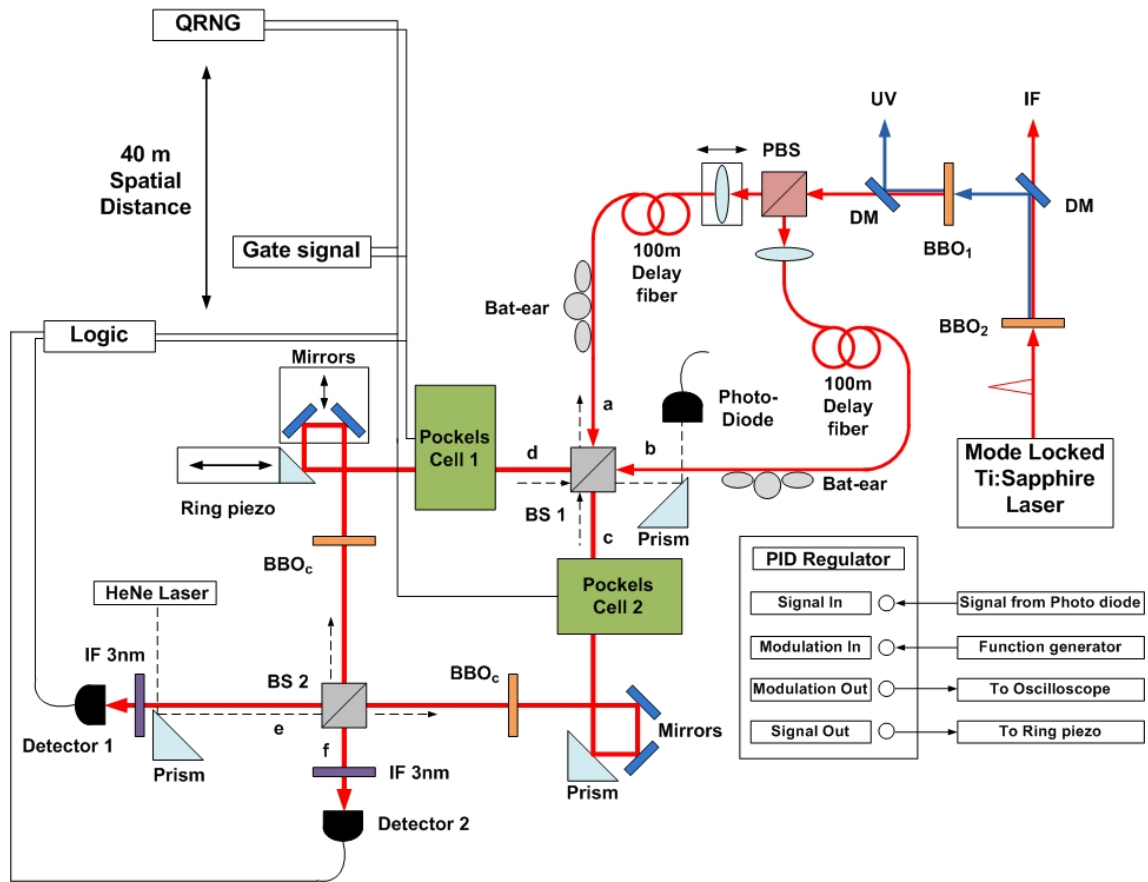
Figure 5.5.: *The setup for the delayed-choice HOM interference experiment. The down-conversion source and the tunable beam splitter are the same as in the previous experiments. The phase of the Mach-Zehnder is zero. When the Pockels Cells are ON and operating at a quarter-wave voltage ($\frac{\pi}{2}$ phase shift) the interferometer works as one big beam splitter. But when they are OFF, the photons pass through the setup and are not interfering at all. The choice-maker is placed 40 m away from the setup. The HOM measurement is performed by measuring the coincidences between det1 and det2 while one fiber coupler at the source is moving through the HOM dip.*

5.2. Conclusion

We experimentally realized a two-photon interference on an interferometric switchable beam splitter. The Pockels Cells inside a Mach-Zehdner interferometer where triggered by a QRNG placed 40 m away from the source. The HOM dip visibility in all three space time scenarios was high enough to exceed the classical limit.

By identifying which photon was switched by the EOMs and which was not we are able to show that complementarity between interference and which way information is also valid in the two photon case. If the Pockels Cells were ON and the MZI operates as a beam
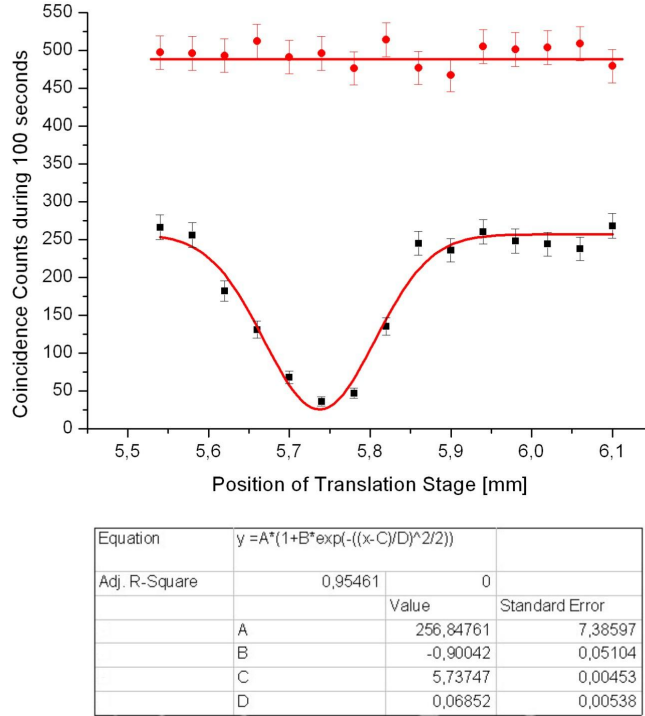
Equation	y =A*(1+B*exp(-((x-C)/D)^2/2))	
Adj. R-Square	0,95461	0
		Value	Standard Error
	A	256,84761	7,38597
	B	-0,90042	0,05104
	C	5,73747	0,00453
	D	0,06852	0,00538

Figure 5.6.: *A measurement result for the delayed-choice HOM dip experiment. The coin-
cidence count rate while the Pockels Cells where ON (black dots) is fitted with
a HOM dip function, which can be seen in the table bellow. The data shows
that the visibility of this dip is $90 \pm 5\%$. In this case we have no which-way in-
formation but high contrast interference. The red dots are the counts while the
EOMs where OFF. In this case no HOM interference shows up and the count
rate is twice as high as the plateau of the dip. In this measurement scenario we
gain precise which-way information and therefore no interference is resolved.
This data shows the results when the choice was space-like separated from the
source (see figure 5.4)*

splitter, high contrast two-photon interference is resolved. But when the Pockels Cells were
OFF and due to the active phase locking inside the MZI, we knew exactly which input
photon was detected in which output mode.

This work significantly extends Wheelers "delayed-choice gedankenexperiment" because
independent from the space-time arrangement between the creation process of the photons
and the setting of the beam splitter, complementarity is valid.

The measurement results also show that our setup is able to realize a fast switchable
Bell-state analyzer as it will be needed for the delayed-choice entanglement swapping
experiment.

6. Outlook - Delayed-Choice Entanglement Swapping

As explained earlier, the main goal of our polarization independent switchable beam splitter is the realization of a delayed-choice entanglement swapping experiment.

First of all I want to introduce the theory which is necessary to understand this experiment. A schematic picture of the setup can be seen in figure 2.5. Two polarization-entangled photon pairs are emitted into 4 spatial modes a, b and c, d respectively. Following the calculations of [29] the initial state can be written as

$$|\Psi\rangle = \frac{1}{\sqrt{2}}(\widehat{a}_H^t\widehat{b}_V^t - \widehat{a}_V^t\widehat{b}_H^t)(\widehat{c}_H^t\widehat{d}_V^t - \widehat{c}_V^t\widehat{d}_H^t)|0\rangle_a|0\rangle_b|0\rangle_c|0\rangle_d \qquad (6.1)$$

Here $\widehat{a}_H^t$ denotes the creation operator acting on mode $|a\rangle$, creating a H polarized photon and $|0\rangle$ indicates the vacuum state. For simplicity I will neglect any global phases and the vacuum states from now on.

Now I want to show how the general state $|\Gamma\rangle = \widehat{b}_x^t\widehat{c}_y^t$, with $x, y \in H, V$, evolves trough the Mach-Zehnder interferometer. The action of a 50:50 beam splitter can be written as

$$\begin{aligned}|a\rangle &\to i|a'\rangle + |b'\rangle \\ |b\rangle &\to |a'\rangle + i|b'\rangle\end{aligned} \qquad (6.2)$$

Therefore the state after the first beam splitter evolves to

$$|\Gamma\rangle = (\widehat{b'}_x^t + i\widehat{c'}_y^t)(\widehat{c'}_x^t + i\widehat{b'}_x^t) \qquad (6.3)$$

Now we include the phase Φ in mode c

$$|\Gamma\rangle = (\widehat{b'}_x^t + i\exp^{i\varphi}\widehat{c'}_y^t)(\exp^{i\varphi}\widehat{c'}_x^t + i\widehat{b'}_x^t) \qquad (6.4)$$

and after the second beam splitter the state becomes to

$$|\Gamma\rangle = [\widehat{b''}_x^t + i\widehat{c''}_x^t + i\exp^{i\varphi}(\widehat{c''}_x^t + i\widehat{b''}_x^t)][i\exp^{i\varphi}(\widehat{c''}_y^t + i\widehat{b''}_y^t) + i(\widehat{b''}_y^t + i\widehat{c''}_y^t)] \qquad (6.5)$$

By substituting $\frac{\varphi}{2} = \Theta$ this can be rewritten as

$$|\Gamma\rangle = -\widehat{b''}^t_x \widehat{b''}^t_y \sin\Theta\cos\Theta - \widehat{b''}^t_x \widehat{c''}^t_y \sin^2\Theta + \widehat{c''}^t_x \widehat{b''}^t_y \cos^2\Theta + \widehat{c''}^t_x \widehat{c''}^t_y \sin\Theta\cos\Theta \qquad (6.6)$$

If we take only those terms were the photons exit into different modes we are left with

$$|\Gamma\rangle = -\widehat{b''}^t_x \widehat{c''}^t_y \sin^2\Theta + \widehat{c''}^t_x \widehat{b''}^t_y \cos^2\Theta \qquad (6.7)$$

With this result we can transform the terms of the initial state 6.1 to the corresponding outputs

$$\widehat{b}^t_V \widehat{c}^t_H \rightarrow -\widehat{b''}^t_V \widehat{c''}^t_H \sin^2\Theta + \widehat{c''}^t_V \widehat{b''}^t_H \cos^2\Theta \qquad (6.8)$$

$$\widehat{b}^t_V \widehat{c}^t_V \rightarrow \widehat{b''}^t_V \widehat{c''}^t_V (\cos^2\Theta - \sin^2\Theta) = \widehat{b''}^t_V \widehat{c''}^t_V \cos 2\Theta \qquad (6.9)$$

$$\widehat{b}^t_H \widehat{c}^t_H \rightarrow \widehat{b''}^t_H \widehat{c''}^t_H \cos 2\Theta \qquad (6.10)$$

$$\widehat{b}^t_H \widehat{c}^t_V \rightarrow -\widehat{b''}^t_H \widehat{c''}^t_V \sin^2\Theta + \widehat{c''}^t_H \widehat{b''}^t_V \cos^2\Theta \qquad (6.11)$$

Therefore the final state becomes to

$$|\Psi\rangle = \widehat{a}^t_H \widehat{d}^t_V (-\widehat{b''}^t_V \widehat{c''}^t_H \sin^2\Theta + \widehat{c''}^t_V \widehat{b''}^t_H \cos^2\Theta) \qquad (6.12)$$

$$- \widehat{a}^t_H \widehat{d}^t_H (\widehat{b''}^t_V \widehat{c''}^t_V \cos 2\Theta) \qquad (6.13)$$

$$- \widehat{a}^t_V \widehat{d}^t_V (\widehat{b''}^t_H \widehat{c''}^t_H \cos 2\Theta) \qquad (6.14)$$

$$+ \widehat{a}^t_V \widehat{d}^t_H (-\widehat{b''}^t_H \widehat{c''}^t_V \sin^2\Theta + \widehat{c''}^t_H \widehat{b''}^t_V \cos^2\Theta) \qquad (6.15)$$

Now I want to think about two special cases

- $\varphi = \Theta = 0$

  In this case the final states looks like

  $$\begin{aligned}|\Psi\rangle &= \widehat{a}^t_H \widehat{d}^t_V \widehat{b''}^t_V \widehat{c''}^t_H - \widehat{a}^t_H \widehat{d}^t_H \widehat{b''}^t_H \widehat{c''}^t_V - \widehat{a}^t_V \widehat{d}^t_V \widehat{b''}^t_H \widehat{c''}^t_H + \widehat{a}^t_V \widehat{d}^t_H \widehat{b''}^t_H \widehat{c''}^t_V \\ &= (\widehat{a}^t_H \widehat{b''}^t_V - \widehat{a}^t_V \widehat{b''}^t_H)(\widehat{c''}^t_H \widehat{d}^t_V - \widehat{c''}^t_V \widehat{d}^t_H)\end{aligned} \qquad (6.16)$$

  which is the initial state. So if the phase in the Mach Zehnder is 0, photons a, b and c'', d'' stay in their original entangled state.

- $\varphi = \frac{\pi}{2} \rightarrow \Theta = \frac{\pi}{4}$

  Here the final state evolves to

  $$\begin{aligned}|\Psi\rangle &= \widehat{a}^t_H \widehat{d}^t_V (-\widehat{b''}^t_V \widehat{c''}^t_H + \widehat{c''}^t_V \widehat{b''}^t_H) + \widehat{a}^t_V \widehat{d}^t_H (-\widehat{b''}^t_H \widehat{c''}^t_V + \widehat{c''}^t_H \widehat{b''}^t_V \\ &= (\widehat{a}^t_H \widehat{d}^t_V - \widehat{a}^t_V \widehat{d}^t_H)(\widehat{b''}^t_H \widehat{c''}^t_V - \widehat{b''}^t_V \widehat{c''}^t_H)\end{aligned} \qquad (6.17)$$

This time we find photons a, d and b'', c'' in an entangled state. By tuning the phase to $\varphi = \frac{\pi}{2}$ the whole Mach-Zehnder interferometer works as a beam splitter and a Bell-state measurement is performed.

Victor is free to choose which type of measurement he wants to perform, but he has to tell Alice and Bob afterwards whether the beam splitter was in or not. In this way Alice and Bob can compare their measurement results and learn from Victor when their photons were in an entangled or separable state.

At the time of writing this thesis, the delayed-choice entanglement swapping experiment was not finished. Therefore I can only present an outlook about what we are going to do. Two polarization-entangled photon pairs are produced by the source described in chapter 3. Our fast interferometrical swichtable beam splitter (chapter 4.1) performs the joint measurement of photons b and c (see figure 6.1). If the Pockels Cells are ON and the Mach-Zehnder interferometer operates as a beam splitter, the entanglement between photons a, b and c, d is swapped to a, d and b, c. But when the Pockels Cells are OFF, the original state produced by the source is preserved and photons a and d remain in a separable product state. The decision whether to put the beam splitter in or not is made randomly by a QRNG (see appendix B) and after photons a and d are already detected and do not longer exist.

The interferometrical switchable beam splitter has to be at the bottom position of the HOM Dip (see chapter 5.1.2) in order to work as a Bell-state analyzer (see appendix C). Since we had problems with the thermal stabilization of our delay fibers in the previous HOM Dip measurements, we placed the fiber spools into a temperature control box. The temperature in the box can be set to a desired degree and is stabilized by a regulation loop. In this way me managed to keep the Dip position stable.

To analyze the polarization of each photon, we used a combination of one quarter-wave plate (QWP) and one half-wave plate (HWP) infront of a polarizing beam splitter (PBS). The two wave plates are used to adjust the measurement basis (H/V, +/-, L/R). The signal of all 8 detectors is send to a coincidence logic and by looking at the 4-fold coincidence events in combination with the ON/OFF signal from the Pockels Cells, we are able to reconstruct the detected state.
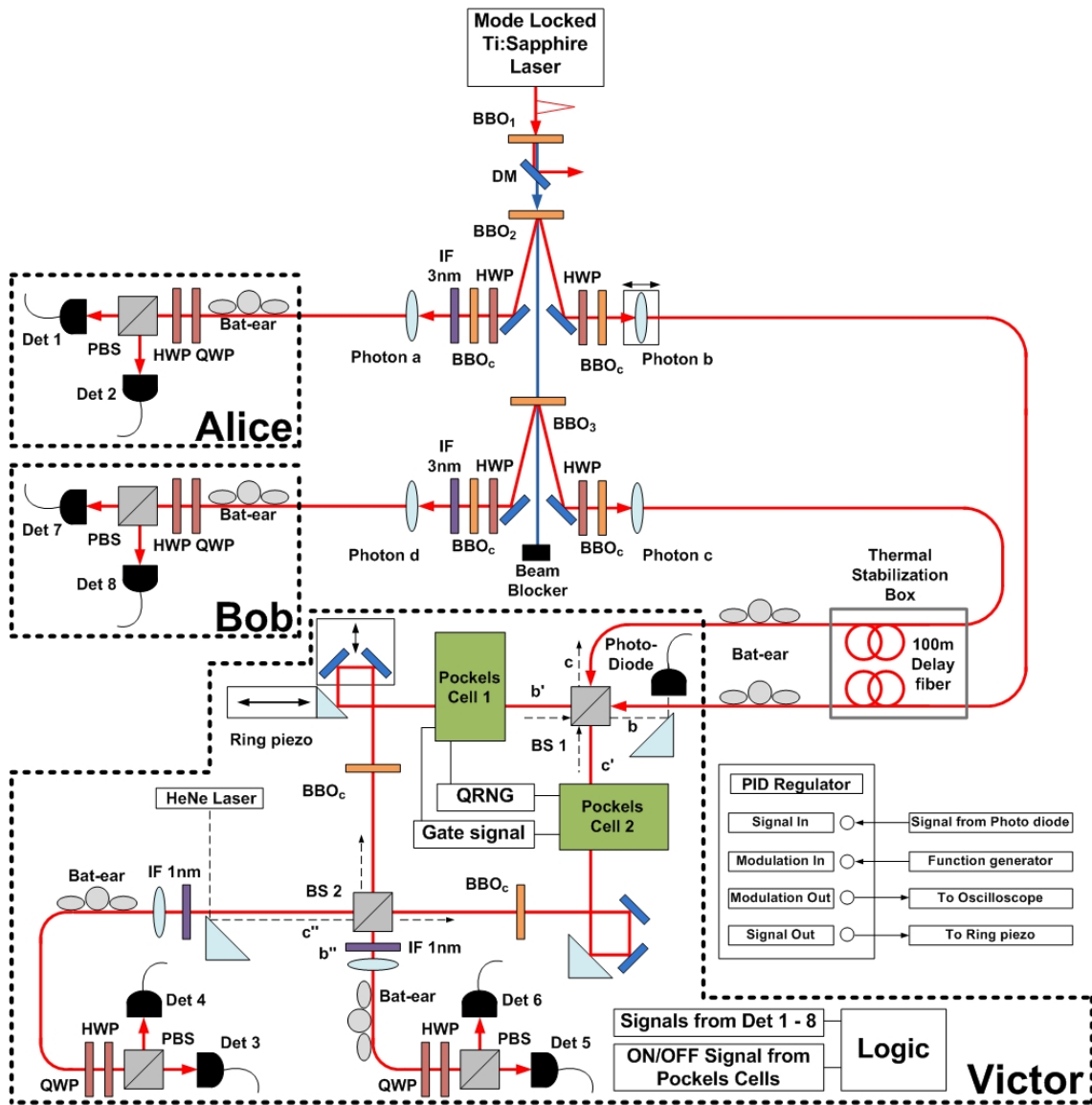
Figure 6.1.: *A schematic diagram of the "delayed-choice entanglement swapping setup". Two polarization-entangled photon pairs are produced from a non-collinear Type-II down-conversion source (for details see chapter 3.1.2). The polarization of photons a and d is measured immediately after their creation. The measurement basis can be adjusted with a combination of one quarter- and one half-wave plate. Photons b and c are delayed with two 100m delay fibers before entering the switchable beam splitter. The polarization inside the single-mode fibers is maintained with Bat-ear polarization controllers and a thermal stabilization box on the 100m fiber. The operation mode of the switchable beam splitter is the same as in the HOM Dip configuration (see chapter 5.1.2). If the Pockels Cells are ON the interferometer works as a Bell-state analyzer, but if the Pockels Cells are OFF, photons b and c pass through the setup without any interaction. Afterwards their polarization is measured as well. The detection events of Alice and Bob are sent to Victor, who, together with his results and the ON/OFF status of the Pockels Cells, is able to reconstruct the detected state. For further details see text and previous chapters.*

7. Conclusion

To summarize my thesis, I have shown a polarization independent ultrafast interferometric switchable beam splitter which can be used for many applications. It consits of a Mach-Zehnder interferometer with one Pockels Cell in each arm. By changing the voltage of the Pockels Cells we can tune the splitting ratio of the effective beam splitter. To test the performance of our setup we used heralded single photons from a collinear spontaneous parametric down-conversion source (SPDC). The switching contrast is above 95% for H/V and +/- polarized photons and the rising time of the Pockels Cells is around 6 ns with a repetition rate of 2.5 MHz. This system represents a useful tool for the scalable linear optical quantum computation and communication.

We have also used the switchable beam splitter to perform a delayed-choice Hong-Ou-Mandel interference experiment under Einstein's locality condition. Both photons of a collinear SPDC source where sent to the two input modes of our modified Mach-Zehnder interferometer. The Pockels Cells where triggered by a quantum random number generator which was located in another lab 40 m away from the photon source and the interferometer. By looking at the coincidence events between the two outputs of the Mach-Zehnder together with the ON/OFF status of the Pockels Cells we were able to resolve two different measurement scenarios. When the Pockels Cells where ON and the interferometer operated as a beam splitter, we observed high contrast two-photon interference. But when the Pockels Cells were OFF and due to the active phase locking inside the MZI, we knew exactly which input photon was detected in which output mode and therefore no interference was resolved. This experiment shows that complementarity between interference and which-way information is also valid for the two-photon case. Furthermore this complementarity is also independent from the space time arrangment between the creation process of the photons and the setting of the beam splitter.

These results show that our setup is able to realize a fast switchable Bell-state analyzer which is needed for a delayed-choice entanglement swapping experiment. This experiment was not finished when I started to write this thesis, but we hope to get some preliminary results soon.

8. Zusammenfassung

In der hier vorliegenden Arbeit werden zwei fundamentale Aspekte der Quantenmechanik behandelt, Verschränkung und Komplementarität. Als Verschränkung bezeichnet man das Phänomen, dass sich zwei oder mehr Teilchen in Superposition befinden können. Jedes einzelne Teilchen des Gesamtsystems ist dabei zu seinen Partnern korreliert, sogar wenn diese räumlich von einander getrennt sind. Das Phänomen der Komplementarität ist eng mit der Heisenberg'schen Unschärferelation verwandt und besagt, dass man zwei Eigenschaften eines Quantenmechanischen Systems nicht gleichzeitig mit beliebiger Genauigkeit messen kann. Ein Beispiel dafür ist der Welle-Teilchen Dualismus.

Die meiste Zeit meiner Diplomarbeit habe ich damit verbracht einen polarisations unabhängigen, ultraschnellen, interferometrisch schaltbaren, Strahlteiler zu realisieren. Dieser besteht aus einem Mach-Zehnder Interferometer welches jeweils eine Pockels Zelle oder elektro-optischen Modulator (EOM) in jedem Arm besitzt. Die EOM's variieren die Phase des transmittierten Strahls indem sie eine Doppelbrechung in einem optischen Kristall mithilfe eines elektrischen Feldes induzieren. Dadurch kann das Verhältnis von Transmission und Reflexion des interferometrischen Stahlteilers geändert werden. Die Effizienz unseres Setups wurde mit Hilfe von verschränkten Photonen Paaren aus einer kollinearen spontaneous parametric down-conversion source (SPDC) getestet. Der Phasenschub Kontrast liegt bei über 95% für Photonen in H/V und +/- polarisations Basis. Die Einschaltzeit der Pockels Zellen beträgt ungefähr 6 ns bei einer Wiederholungsrate von 2.5 MHz. Dieses System stellt ein nützliches Werkzeug für optische Quantencomputer oder Quantenkommunikation dar.

Weiters haben wir den schaltbaren Strahlteiler benutzt um ein delayed-choice Hong-Ou-Mandel Interferenz Experiment unter Einstein'schen Lokalitätsbedingungen durchzuführen. Beide Photonen einer kollinearen SPDC Quelle wurde zu den beiden Eingängen des modifizierten Mach-Zehnder Interferometers geschickt. Die Pockels Zellen wurden von einem Quanten Zufallszahlen Generator gesteuert welcher sich in 40 m Entfernung von unserem Labor befand. Wir betrachteten die Koinzidenzen zwischen den beiden Ausgängen des Interferometers in Kombination mit dem ON/OFF Status der Pockels Zellen. Dadurch waren wir in der Lage zwei verschiedene Messungen gleichzeitig durchzuführen. Wenn die Pockels Zelle auf ON gestellt war und das Interferometer dadurch als Strahlteiler fungierte, konnten wir zwei-Photonen Interferenz in der Koinzidenz Messung sehen. Waren die Pockels Zellen

jedoch auf OFF gestellt, wussten wir Aufgrund der aktiven Phasen Kontrolle innerhalb des Mach-Zehnders, genau welches Eingangsphoton welchen Ausgang genommen hatte. Aufgrund dieser "welcher-Weg" Information lässt sich in diesem Fall keine Interferenz feststellen. Die Messergebnisse zeigen, dass die Komplementarität zwischen Interferenz und "welcher-Weg" Information auch in einem zwei-Photonen Experiment gültig ist. Ausserdem ist diese Komplementarität unabhängig von der raum-zeitlichen Anordnung zwischen dem Enstehungsprozess der Photonen und der Entscheidung welches Experiment durchgeführt werden soll.

All diese Ergebnisse zweigen, dass dieses Setup in der Lage ist eine schnelle, schaltbare Bell-Zustandsmessung durchzuführen, wie es für ein delayed-choice entanglement swapping Experiment nötig ist. Leider ist dieses Experiment noch nicht beendet, aber wir hoffen, dass wir bald die ersten Messungen durchführen können.

A. Single-Photon Integrating Spectrometer

For our quantum information experiments with photons, precise knowledge about the spectral properties of the used single photons is obligatory. But since a commercial spectrometer with high sensitivity is very large and expensive, we had do design our own. One important aspect of our self built spectrometer is to avoid usage of any slits in the light beam, hence achieving maximum photon transmission.

For single photon detection one can either use an Avalanche Photo Diode (APD) or a CCD chip with a very long integration time[1]. Since we had a very good CCD camera from the company *Meade Instruments Corporation* called *Deep Sky Imager* which is actually used for astronomic telescopes, we decided to design our spectrometer with this camera. The exposure time of the CCD chip can be adjusted from 1 ms up to 1 hour, which allows us to measure the spectrum of a strong laser pulse as well as single photons.

A picture of our setup can be seen in figure A.1. The beam spreads out from a single-mode fiber, which is used to guide the single photons into the spectrometer and is collimated afterwards with a 75 mm lens. The collimated beam has a diameter of 18,4 mm and is centered on a blazed reflection grating.

A blazed diffraction grating (see figure A.2) has the advantage that no light is lost in the 0th order, like it is for a normal grating. In addition a blazed grating gives you the opportunity to scan a wide range of wavelengths. But it has to be kept in mind that only for a specific wavelength the blazing condition is fullfiled. Outside of this region the efficiency drops dramatically and the advantage of a blazed configuration is not given any more. Our grating is from the company *Thorlabs Inc.* and has a blazing angle of 13° with 1200 grooves per mm. The center wavelength is at 750 nm which is close enough to 808 nm (our Laser wavelength) to fullfil the blazing condition.

The diffracted beam is focused with a 50 mm lens onto the CCD camera. Each pixel has a size of $8,3x8,6\mu m$ and gives an 8-bit output value which depends on the recorded intensity. The data is stored in .jpg files and can be used for further analysis see figure A.3. The intensity distribution for each pixel line is exported and fitted with a Gaussian function (see figure A.4). These plots correspond to the frequency distribution of the

---

[1]A spectrometer which makes use of an APD detector was build by my colleague Bibiane Blauensteiner and is described in her diploma thesis [50].
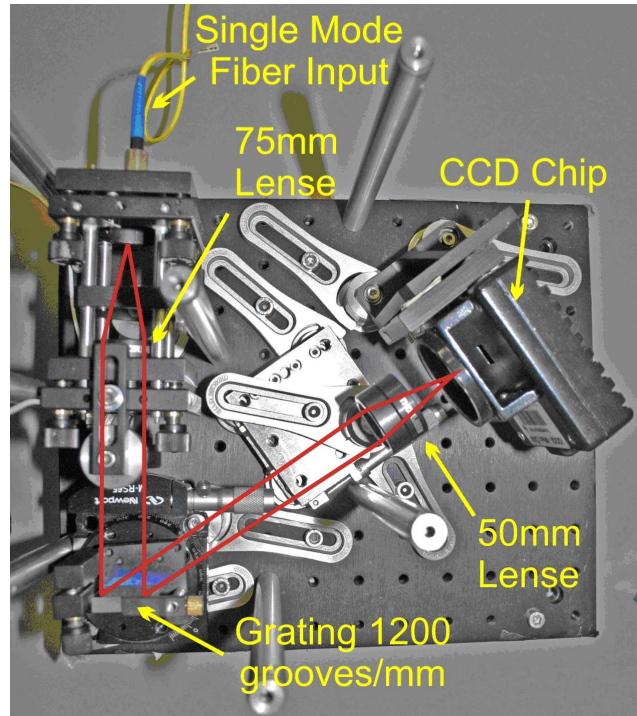
Figure A.1.: *A picture of the single photon integrating spectrometer. The beam spreads out from a single-mode fiber and is collimated by a 75mm lens. Afterwards it gets diffracted by a blazed grating and is focused onto a CCD chip. The setup was enclosed with a box to isolate it from ambient light. For further details see text.*
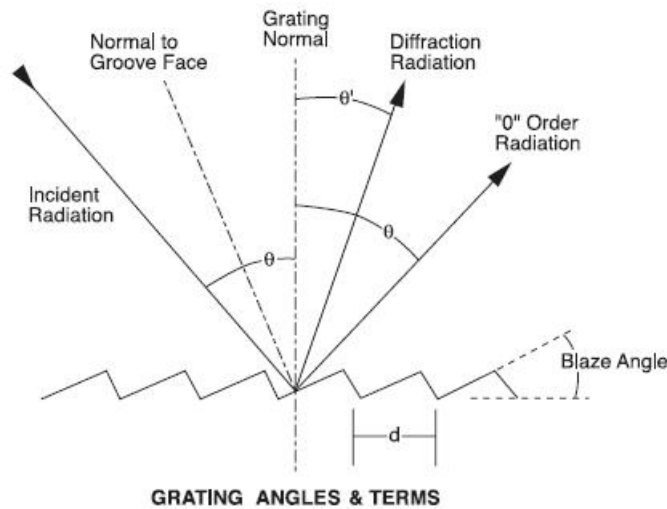

Figure A.2.: *A schematic picture of a blazed diffraction grating. Picture taken from http://www.thorlabs.com/catalogPages/800.pdf*

incoming light. The fitting results like FWHM and center peak are given in units of pixels. In order to gain knowledge out of these numbers we have to calibrate our spectrometer.

Figure A.3.: *A spectrogram picture taken by the Deep Sky Imager CCD Camera. It shows the spectrum of a 4nm interference filter at 810nm. The number of illuminated pixels in the horizontal axis depends on the spectral width of the diffracted beam.*
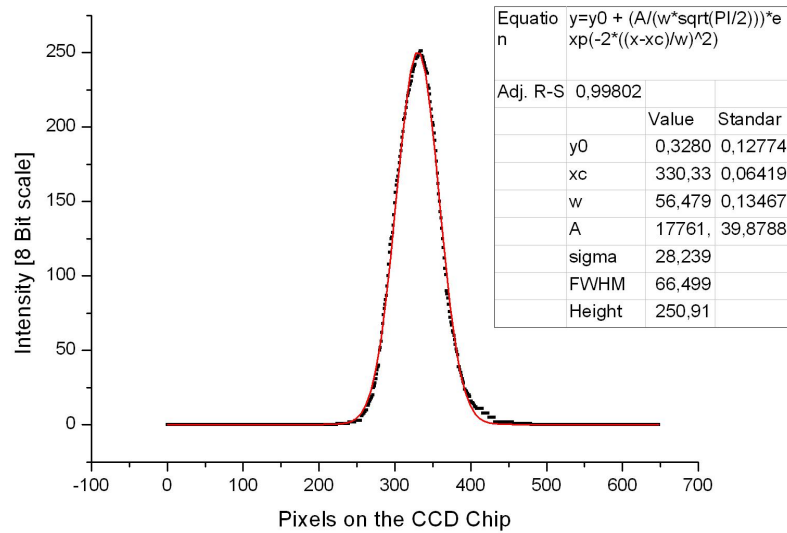

Figure A.4.: *The measurement data from figure A.3 is imported into an analysis program and fitted with a Gaussian function. The fitting data shows the central peak and FWHM in units of pixels. From those values we are able to calculate the center wavelength and FWHM in nm.*

The calibration was done by using the well known spectral properties of several interference filters. We placed them into the collimated beam, before the grating and measured the central frequency and FWHM in units of pixels with our spectrometer. The results were plotted against the known bandwidth of the filters and fitted with a linear function (see figure A.5). The slope of the linear regression tells us that 1 pixel corresponds to $0,083 \pm 0,002nm$. The offset of $-0,89 \pm 0,09nm$ would mean that even a beam of 0nm bandwidth (no input) illuminates approximately 11 pixel. This is not physical and therefore we know that the spectrum gets broadened inside our spectrometer due to bad alignment, lens errors or irregularities on the grating.
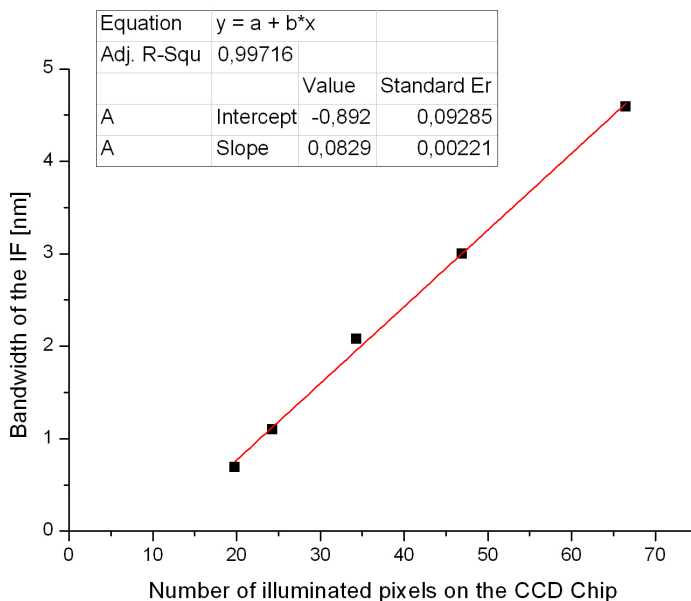
Figure A.5.: *The measurement data from several different IF's was fitted with linear regression to calibrate the spectrometer. The slope tells us that 1 pixel corresponds to $0,083 \pm 0,002 nm$. The offset is a result of alignment errors, lense errors or irregularities on the grating.*

Another explanation would be that the width of the interference filters is actually larger than we believe. But this can be ruled out since we checked their spectral properties with a commercial spectrometer called *Perkin Elmer Lambda 950 UV/VIS Spectrometer*. The measurement results fit the values of the company's data sheet[2] within measurement errors.

Figure A.6 shows the spectral properties of our collinear down-conversion source. Due to our calibration, the FWHM can be calculated by $164(FWHM\ in\ pixel) * 0,083 - 0,89 = 12,7 \pm 0,4 nm$. The central bandwidth was found by comparing the peak transmission of our 810nm filters with the measurement result of the down-conversion photons. Therefore the maximum of plot A.6 is at $811,2 \pm 1,0 nm$.

---

[2]The IF filters are purchased from the company *Lot Oriel*.

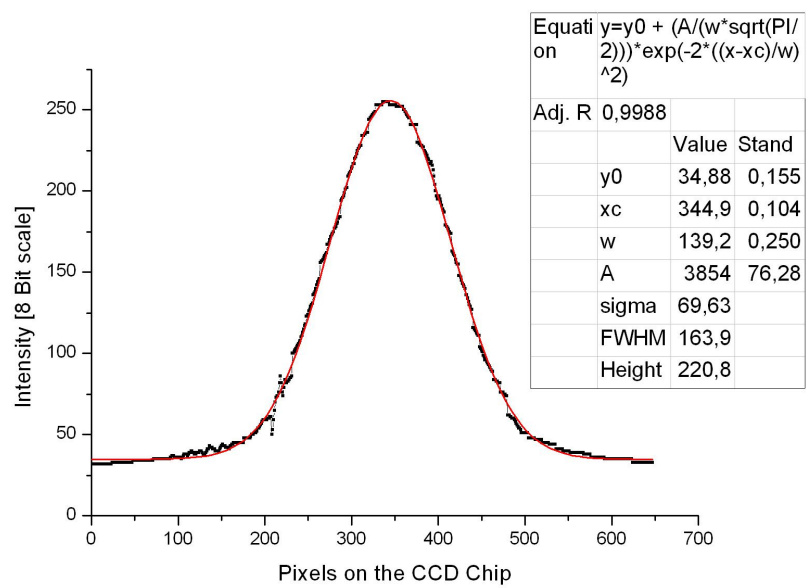| Equation	y=y0 + (A/(w*sqrt(PI/2)))*exp(-2*((x-xc)/w)^2)	
Adj. R	0,9988	
	Value	Stand
y0	34,88	0,155
xc	344,9	0,104
w	139,2	0,250
A	3854	76,28
sigma	69,63	
FWHM	163,9	
Height	220,8	

Figure A.6.: *The spectrum of the photons from our collinear down-conversion source (ordinary beam). From this intensity distribution plot we can calculate that the beam has a central peak at $811,2 \pm 1,0nm$ with a FWHM of $12,7 \pm 0,4nm$. The exposure time of the camera for this measurement data was around 20 minutes.*

B. Quantum Random Number Generator

In our experiments the complete randomness of the action of the Pockels Cells has to be guaranteed. It is important that, not even in principle, any information of the projection process done by the On state of the Pockels Cells, can influence the state produced at the source.

The quantum random number generator we used was introduced by T. Jennewein et al. in 2000 [51]. The system is based on the quantum physical prediction that a photon entering a 50:50 beam splitter, has equal probability to get reflected or transmitted (see figure B.1). Fast photon detectors in the outputs trigger a toggle switch which creates a binary random signal (see figure B.2). The switch is set to 0 if detector 1 clicks and remains in this state until detector 2 fires. In our experiments the QRNG was operating at 34,8 MHz with an autocorrelation time of 11,8 ns (see figure B.3).
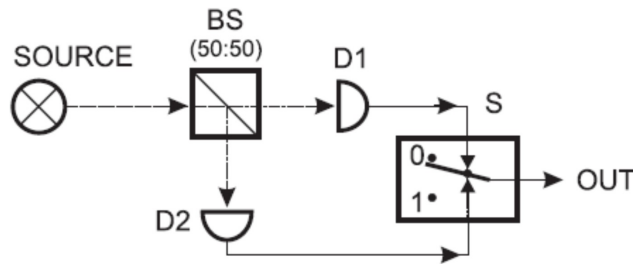

Figure B.1.: *Operation principle of Quantum Random Number Generator. A weak light beam from a LED is split on a 50:50 beam splitter. The detection events in each output mode trigger a toggle switch which produces a binary random signal. Picture taken from [51].*

In order not to damage our Pockels Cells we gated the random signal from the QRNG with a 2,5 MHz ramp signal from a function generator. This corresponds to a duty cycle of $0,4\mu s$ which is more than two orders of magnitude larger than the autocorrelation time of the QRNG. Therefore we can exclude the prediction of the present signal from the last one. And to rule out that any choice related event is able to influence the status of our single photons, by some hidden communication (slower than the speed of light), we generalize the random number decision to a series of events. We include three times the autocorrelation time of 11,8 ns and the internal delay of the QRNG (around 75 ns). Therefore the choice, drawn in the space time diagramm (see figure 5.4), is a series of events lasting for 110 ns.
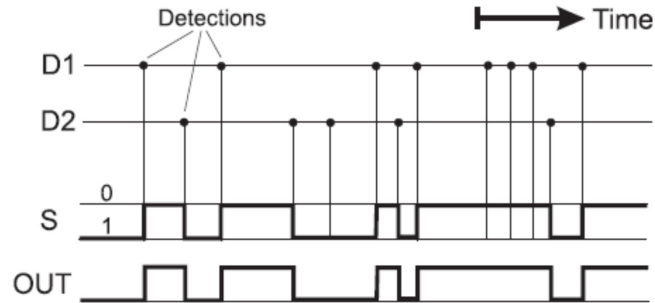
Figure B.2.: *A successful detection event on detector 1 sets the toggle switch to 0. The status remains 0 until detector 2 fires and the signal is switched to 1. Picture taken from [51].*
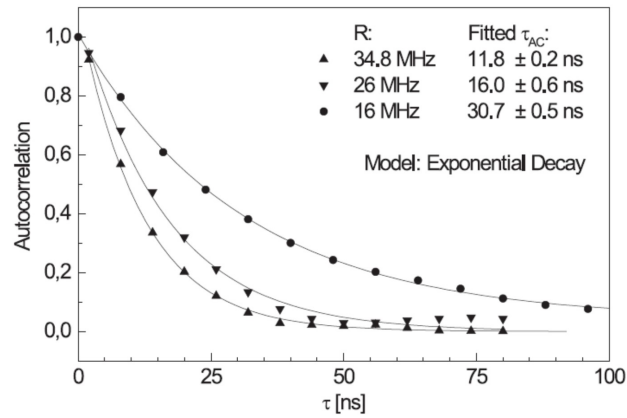

Figure B.3.: *The autocorrelation functions are calculated from traces of the random signal for different frequencies. The data is fitted with a exponential decay function. Picture taken from [51].*

C. Bell-state Analyzer

A Bell-state analyzer is used to identify in which of the four Bell-states the two entangled input photons are. Today, no perfect Bell-state analyzer is available, but by exploiting the photon statistic of a two-photon interference on a 50:50 beam splitter, one can identify two out for Bell-states. A detailed calculation for this can be found in [41].

Imagine a 50:50 beam splitter with two input modes a, b and two output modes c, d. The action of this beam splitter can be written as

$$
\begin{aligned}
|a\rangle &\rightarrow \frac{i}{\sqrt{2}}|c\rangle + \frac{1}{\sqrt{2}}|d\rangle \\
|b\rangle &\rightarrow \frac{1}{\sqrt{2}}|c\rangle + \frac{i}{\sqrt{2}}|d\rangle
\end{aligned}
\tag{C.1}
$$

As an input state we choose the $|\Psi^-\rangle = \frac{1}{\sqrt{2}}(\widehat{a}_H^t \widehat{b}_V^t - \widehat{a}_V^t \widehat{b}_H^t)|0\rangle$ Bell-state. Here $\widehat{a}_H^t$ denotes the creation operator acting on mode a, creating a H polarized photon and $|0\rangle$ indicates the vacuum state. If the two entangled photons are indistinguishable in every degree of freedom, then the state after the beam splitter evolves to

$$
|\Psi^-\rangle_{cd} = \frac{1}{2\sqrt{2}}[(i\widehat{c}_H^t + \widehat{d}_H^t)(\widehat{c}_V^t + i\widehat{d}_V^t) - (i\widehat{c}_V^t + \widehat{d}_V^t)(\widehat{c}_H^t + i\widehat{d}_H^t)]|0\rangle
\tag{C.2}
$$

This can be summarized to

$$
|\Psi^-\rangle_{cd} = \frac{1}{\sqrt{2}}(\widehat{c}_V^t \widehat{d}_H^t - \widehat{c}_H^t \widehat{d}_V^t)|0\rangle
\tag{C.3}
$$

One can see that the photons always exit in distinct modes with different polarization. If we choose a $|\Psi^+\rangle$ input, the same calculation shows that both photons will always exit into the same spatial mode having opposite polarization, see figure C.1. To identify a $|\Phi^\pm\rangle$ state one would have to use a photon number counting detector, because they will always be found in the same exit having same polarization.

By using a combination of one beam splitter and two polarizing beam splitters we can identify two out four Bell-states by looking at the coincidence detection events between the four output detectors.
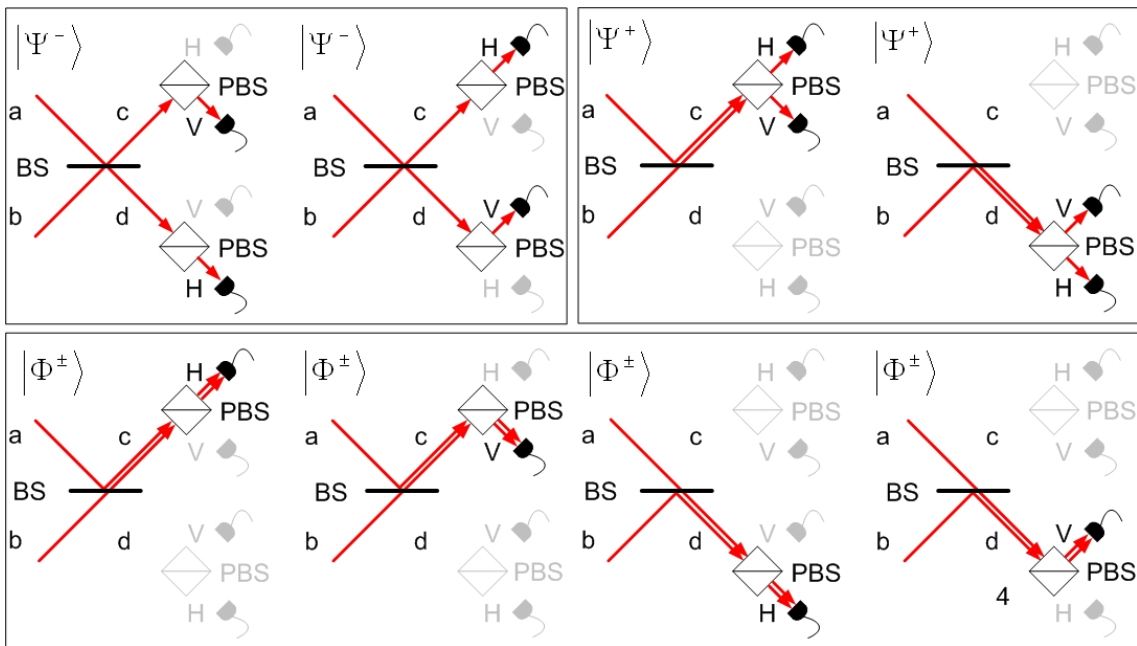
Figure C.1.: *This schematic diagram shows the possible outcomes of photon detections for all four Bell-states entering a 50:50 beam splitter. The polarization of the photons are analyzed with a PBS in each arm. Clearly two out of four Bell-states can be identified perfectly (Ψ^- and Ψ^+). The remaining two ($|\Phi^\pm\rangle$) can only be identified together in this setup.*

Bibliography

[1] A. Einstein, B. Podolsky, and N. Rosen. Can quantum-mechanical description of physical reality be considered complete? *Physical Review Letter*, 47:777–780, 1935.

[2] J. A. Wheeler and W. H. Zurek. *Law Without Law*, page 184. Princeton University Press, 1983.

[3] John Steward Bell. On the Einstein Podolsky Rosen paradox. *Physics*, 1:195–200, 1964.

[4] A. Peres. Delayed choice for entanglement swapping. *J. Mod. Optic*, 47:139, 2000.

[5] C. Brukner, M. Aspelmayer, and A. Zeilinger. Complementarity and information in "delayed-choice for entanglement swapping". *http://arxiv.org/abs/quant-ph/0405036v1*, 2004.

[6] G. Möllenstedt and C. Jönsson. Elektronen-Mehrfachinterferenzen an regelmäßig hergestellten Feinspalten. *Zeitschrift für Physik*, 155:472–474, 1959.

[7] A. Zeilinger, R. Gähler, C. G. Shull, W. Treimer, and W. Mampe. Single- and double-slit diffraction of neutrons. *Rev. Mod. Phys.*, 60:1067–1073, 1988.

[8] O. Carnal and J. Mlynek. Young's double-slit experiment with atoms: A simple atom interferometer. *Physical Review Letter*, 66:2689–2692, 1991.

[9] M. Arndt, O. Nairz, J. Vos-Andreae, C. Keller, G van der Zouw, and A. Zeilinger. Waveparticle duality of C60 molecules. *Nature*, 401:680–682, 1999.

[10] T. Hellmuth, H. Walther, A. Zajonc, and W. Scheich. Delayed-choice experiments in quantum interference. *Physical Review Letter*, A35:2532–2541, 1987.

[11] J. Baldzuhn, E. Mohler, and W. Martienssen. A wave-particle delayed-choice experiment with a single-photon state. *Zeitschrift für Physik B*, 77:347–352, 1989.

[12] V. Jacques, E. Wu, F. Grosshans, F. Treussart, P. Grangier, A. Aspect, and J. F. Roch. Experimental realization of Wheeler's delayed-choice gedanken experiment. *Science*, 315:966–968, 2007.

[13] S. Dürr, T. Nonn, and G. Rempe. Fringe visibility and which-way information in an atom interferometer. *Physical Review Letter*, 81:5705–5709, 1998.

[14] E. Schrödinger. Die gegenwärtige Situation in der Quantenmechanik. *Naturwissenschaften*, 23:807–812; 823–828;844–849, 1935.

[15] Albert Einstein. *Albert Einstein, Philosopher Scientist*, page 85. edited by P.A. Schlipp, 1949.

[16] Niels Bohr. Can quantum-mechanical description of physical reality be considered complete? *Physical Review Letter*, 48:696–702, 1935.

[17] J. F. Clauser, M. A. Horne, A. Shimony, and R. A. Holt. Proposed experiment to test local hidden-variable theories. *Physical Review Letter*, 23:880–884, 1969.

[18] J. F. Clauser and A. Shimony. Bell's theorem: experimental tests and implications. *Rep. Prog. Phys.*, 41:1881, 1978.

[19] A. Aspect, P. Grangier, and G. Roger. Experimental realization of Einstein-Podolsky-Rosen-Bohm gedankenexperiment: A new violation of Bell's inequalities. *Physical Review Letter*, 49:91–94, 1982.

[20] G. Weihs, T. Jennewein, C. Simon, H. Weinfurter, and A. Zeilinger. Violation of Bell's inequality under strict Einstein locality conditions. *Physical Review Letter*, 81:5039–5043, 1998.

[21] M. A. Rowe, D. Kielpinski, V. Meyer, C. A. Sackett, W. M. Itano, C. Monroe, and D. J. Wineland. Experimental violation of a Bell's inequality with effcient detection. *Nature*, 409:791–794, 2001.

[22] C. H. Bennett, G. Brassard, C. Cr'epeau, R. Jozsa, A. Peres, and W. K.Wootters. Teleporting an unknown quantum state via dual classical and Einstein-Podolsky-Rosen channels. *Physical Review Letter*, 70 (13), 1993.

[23] D. Bouwmeester, J.-W. Pan, K. Mattle, M. Eibl, H. Weinfurter, and A. Zeilinger. Experimental quantum teleportation. *Nature*, 390:575–579, 1997.

[24] Jian-Wei Pan. *Quantum Teleportation and Multi-photon Entanglement*. PhD thesis, Universität Wien, 1998.

[25] M. Zukowski, A. Zeilinger, M. A. Horne, and A. K. Ekert. "event-ready-detectors" Bell experiment via entanglement swapping. *Physical Review Letter*, 71:4287–4290, 1993.

[26] J. W. Pan, D. Bouwmeester, H. Weinfurter, and A. Zeilinger. Experimental entanglement swapping: Entangling photons that never interacted. *Physical Review Letter*, 80:3891–3894, 1998.

[27] Thomas Jennewein. *Quantum Communication and Teleportation Experiments using Entangled Photon Pairs*. PhD thesis, Universität Wien, 2002.

[28] T. Jennewein, G. Weihs, J. W. Pan, and A. Zeilinger. Experimental nonlocality proof of quantum teleportation and entanlement swapping. *Physical Review Letter*, 88:017903, 2002.

[29] T. Jennewein, C. Brukner, M. Aspelmayer, and A. Zeilinger. Experimental proposal of switched "delayed-choice" for entanglement swapping. *International Journal of Quantum Information*, 3:73–79, 2005.

[30] H. Takesue, H. Fukuda, T. Tsuchizawa, T. Watanabe, K. Yamada, Y. Tokura, and S.-I. Itabashi. Generation of polarization entangled photon pairs using silicon wire waveguide. *Optics Express*, 16:5721–5727, 2008.

[31] A. Martin, V. Cristofori, P. Aboussouan, H. Herrmann, W. Sohler, D. B. Ostrowsky, O. Alibart, and S. Tanzilli. Integrated optical source of polarization entangled photons at 1310 nm. *Optical Express*, 17:1033–1041, 2009.

[32] B. S. Shi and A. Tomita. Generation of a pulsed polarization entangled photon pair using a Sagnac interferometer. *Physical Review Letter*, 69:013803, 2004.

[33] A. Fedrizzi, T. Herbst, A. Poppe, T. Jennewein, and A. Zeilinger. A wavelength-tunable fiber-coupled source of narrowband entangled photons. *optics Express*, 15:15377–15386, 2007.

[34] X.-H. Bao, Y. Qian, J. Yang, H. Zhang, Z.-B. Chen, T. Yang, and J.-W. Pan. Generation of narrow-band polarization-entangled photon pairs for atomic quantum memories. *Physical Review Letter*, 101:190501, 2008.

[35] P. Kwiat, K. Mattle, H. Weinfurter, and A. Zeilinger. New high-intensity source of polarization-entangled photon pairs. *Physical Review Letter*, 75, 1995.

[36] J. G. Rarity and P. R. Tapster. Experimental violation of Bell's inequality based on phase and momentum. *Physical Review Letter*, 64:2495–2498, 1990.

[37] J. Brendel, N. Gisin, W. Tittel, and H. Zbinden. Pulsed energy-time entangled twin-photon source for quantum communication. *Physical Review Letter*, 82:2594–2597, 1999.

[38] D. Bouwmeester, A. Ekert, and A. Zeilinger. *The Physics of Quantum Information*. Springer Verlag, 2000.

[39] W. Tittel and G. Weihs. Photonic entanglement for fundamental tests and quantum communication. *arXiv.org*, arXiv:quant-ph/0107156v1, 2001.

[40] Gregor Weihs. *Ein Experiment zum Test der Bellschen Ungleichung unter Einsteinscher Lokalität*. PhD thesis, Universität Innsbruck, 1999.

[41] Klaus Mattle. *Nichtklassische Lichtzustände zur Optischen Nachrichtenübertragung*. PhD thesis, Universität Innsbruck, 1997.

[42] Nuray Tetik. Delayed-choice experiments with entangled photons. Diploma thesis, University of Vienna, 2007.

[43] Friedrich Pockels. Abhandlungen der Koeniglichen Gesellschaft der Wissenschaften zu Goettingen. 39, 1894.

[44] B. E. A. Saleh and M. C. Teich. *Fundamentals of Photonics*. John Wiley & Sons, Inc., 1991.

[45] Rainer Kaltenbaek. Active switching in long distance quantum state teleportation. Master's thesis, Universität Wien, 2003.

[46] R. Prevedel, P. Walther, F. Tiefenbacher, P. Böhi1, R. Kaltenbaek, T. Jennewein, and A. Zeilinger. High-speed linear optics quantum computing using active feed-forward. *Nature*, 445:65–69, 2007.

[47] C. K. Hong, Z. Y. Ou, and L. Mandel. Measurement of subpicosecond time intervals between two photons by interference. *Physical Review Letter*, 59, 1987.

[48] R. Ghosh and L. Mandel. Observation of nonclassical effects in the interference of two photons. *Physical Review Letter*, 59:1903–1905, 1987.

[49] Rainer Kaltenbaek. *Entanglement Swapping and Quantum Interference with Independent Sources*. PhD thesis, Universität Wien.

[50] B. Blauensteiner. A single-photon spectrometer for quantum optics experiments with independent sources. Master's thesis, Technische Universität Wien.

[51] T. Jennewein, U. Achleitner, G. Weihs, H. Weinfurter, and A. Zeilinger. A fast and compact quantum random number generator. *Review of Scientific Instruments*, 71, 2000.

D. Acknowledgments

First of all I want to thank Prof. Anton Zeilinger for giving me the opportunity to work on this project and for creating this unique research environment.

I also want to thank my supervisor Thomas Jennewein for helping us with so many problems in the lab and for all the calculation and simulations he did on our experiment. Without his priceless ideas and tremendous input we would have not been able to finish this experiment.

My deepest appreciation goes to my lab mate Xiao-song Ma who was never too tired to help me with any problem or to answer my stupid questions. He teached me a lot about experimental work and physics in general. But especially I want to thank him for the nice working climate, for all the fun we had and for being a good friend.

I also want to thank every one else in the group for their help and for the pleasant atmosphere.

My last acknowledgments go to my friends and family and therefore I want to switch to my mother tongue german.

Ich möchte all meinen Freunden und Bekannten dafür danken, dass sie mich nach einem langen Tag in der Quanten Welt immer wieder in die klassische Welt zurückgeholt haben. Sicher war es nicht leicht meine langen und teilweise unverständlichen Vorträge über Physik zu ertragen, aber ihr habt es immer wieder geschafft mich daran zu erinnern, dass es auch noch andere schöne Dinge im Leben gibt.

Meinen Großeltern möchte ich ganz besonders dafür danken, dass sie mich während meines Studiums finanziell unterstützt haben, wodurch ich mich voll und ganz auf die Physik konzentrieren konnte.

Ein liebevolles Dankeschön geht auch an meine Freundin Caroline. Sie hat es nicht nur geschafft meine langen Arbeitszeiten und meinen Perfektionismus zu ertragen, sondern auch mich jeden Tag aufs Neue unglaublich glücklich zu machen.

Und zu guter Letzt möchte ich meinen liebevollen Eltern danken. Ihr habt mich Zeit meines Lebens gefördert und mich bei jeder Entscheidung unterstützt. Danke für alles!

E. Curriculum Vitae

Personal Data

Name: Stefan Zotter

Born: 20.09.1984 Vienna, Austria

Parents: Werner and Andrea Zotter

Chronology

1991-1995: Volksschule (Primary School) Wien

1995-2003: Realgymnasium (Highschool) BRG. 19 Krottenbachstraße, Wien

06.2003: Matura

09.2003-04.2004: Obligatory military service with the Austrian Army at Landesverteidigungsakademie Wien

10.2004-03.2008: Study of Physics at the University of Vienna

2002-2007: Several internships at Siemens Business Services Gmbh &Co (4x times) and Andritz AG (7x times)

03.2008-now: Diploma Thesis in Experimental Physics and Researcher at the Institute for Quantum Optics and Quantum Information, Austrian Academy of Science